RSC Advances

REVIEW

View Article Online
View Journal | View Issue

Cite this: *RSC Adv.*, 2023, **13**, 17787

The role of lanthanide luminescence in advancing technology

Gabriella Tessitore, †*[ab] Gabrielle A. Mandl, †[a] Steven L. Maurizio, [a] Mannu Kaur [a] and John A. Capobianco *[a]

Our society is indebted to the numerous inventors and scientists who helped bring about the incredible technological advances in modern society that we all take for granted. The importance of knowing the history of these inventions is often underestimated, although our reliance on technology is escalating. Lanthanide luminescence has paved the way for many of these inventions, from lighting and displays to medical advancements and telecommunications. Given the significant role of these materials in our daily lives, knowingly or not, their past and present applications are reviewed. A majority of the discussion is devoted to pointing out the benefits of using lanthanides over other luminescent species. We aimed to give a short outlook outlines promising directions for the development of the considered field. This review aims to provide the reader enough content to further appreciate the benefits that these technologies have brought into our lives, with the perspective of travelling among the past and latest advances in lanthanide research, aiming for an even brighter future.

Received 13th February 2023
Accepted 30th May 2023

DOI: 10.1039/d3ra00991b

rsc.li/rsc-advances

1 Introduction

For a long time after their discovery, lanthanides did not initially find a suitable application, despite their far-reaching technological use in our quotidian.[1–4] The first real barrier to any practical use of such elements was their similar ionic radii in their most common trivalent form. Their similar sizes impacted each step of their discovery process, even during the initial attempts to simply identify the whole lanthanide series upon their extraction from minerals like gadolinite, first discovered in the 1790s. Due to the similarities between these elements, some of their mixtures were initially confused for a single new element. It took almost two centuries of research to finally confer these elements their rightful place on the periodic table.

Their reputation as rare earths is also somewhat misleading. Most of the lanthanides are indeed among the least abundant metals on Earth, but they are all more abundant than gold.[5] Moreover, the presence of some of the lanthanides in minerals is far from scarce, such as cerium, neodymium and lanthanum. Cerium is almost as abundant as zinc, which is considered a relatively abundant element. The label "rare" confers a sense of preciousness to the lanthanides, which is well represented by their relatively high cost compared to other elements of similar abundance. Because lanthanides are not concentrated in a single ore, their extraction is difficult, resulting in supply chain disruptions in past decades.[6] These factors, more than their relative abundance, brought about a sense of uncertainty in the industries relying on them. This uncertainty, in combination with their relatively high cost, resulted in industries seeking out alternative elements.

Financial factors have a significant impact on the commercialization of a novel technology. From a cost-benefit aspect, the inclusion of lanthanides into otherwise affordable and functioning technologies might not represent an advisable route to improving them. For example, cost-benefit concerns for using lanthanides are probably not a significant issue for a billion-dollar aerospace mission, while the benefits achieved by a lanthanide-based photocatalyst in wastewater treatments may not be enough to counterbalance the cost of the proposed purification system. This review focuses on applications in which the technologies benefitting from lanthanide luminescence reached widespread commercial use.

Despite their drawbacks, lanthanides are part of multiple inventions which have become essential in modern society.[7–11] More common applications of the pure lanthanide metals are in metallurgy, ceramics, and catalysis, while the magnetic and optical properties of the di-, tri- and tetravalent ions are exploited in various industries. The versatility of lanthanide-based luminescent materials in terms of the possible excitation sources and luminescence wavelengths, lifetimes and band characteristics explains the reasons behind their broad use in many fields that rely on light.[12–15] Extensive reviews about the

[a]*Concordia University, Department of Chemistry and Biochemistry & Center for NanoScience Research, 7141 Rue Sherbrooke Ouest, Montreal, QC, Canada. E-mail: john.capobianco@concordia.ca*

[b]*Department of Chemistry, Université Laval, 1045 Av. de la Médecine, Québec, QC, G1V 0A6 Canada. E-mail: gabriella.tessitore@chm.ulaval.ca*

† Gabriella Tessitore and Gabrielle A. Mandl contributed equally to the preparation of the manuscript (co-first authors).

luminescence mechanisms of lanthanide ions in different oxidation states can be found elsewhere.[7,10]

Importantly, the reported technologies are in actual use or, at minimum, their use in patented prototypes has already been demonstrated. Although there are many prospective new technologies reported in the academic literature that may one day become staples in future society, the aim of this review is to outline the advancements that have made our current lanthanide-based technologies possible. Nevertheless, prospective promising applications are provided for each section. Finally, we provide in-depth descriptions only of technologies relevant to modern times, with the ambition to inspire the future of the field by providing the most successful examples of our era.

2 Lanthanides in lighting and displays

2.1 Early uses of phosphors: incandescence, fluorescence and cathodoluminescence

The beginning of the modern era is often thought to coincide with the advent of artificial, or electric, illumination in the 19th century. The creation of the first light bulb was developed by Joseph Wilson Swan, and improved upon by the likes of Edison, Thompson, and Tesla among others.[16] The electric arc light was also introduced around this time.[17]

Simultaneously, there were other types of electrical lighting being explored, as the efficiency of the incandescent lamp is limited by its own resistive nature: incandescence occurs by thermal conversion of electricity caused by the resistance of the material. Thus, much of the energy is dissipated as heat rather than light. Electrical lighting based on gas-discharge was first observed during the 17th century and was continually studied and improved upon because of its higher efficiency than incandescence.[18] Moreover, the invention of the discharge lamp resulted in less dissipative and more efficient light conversion, at the initial disadvantage of producing light at hues not suitable for indoor illumination.[19] For example, mercury lamps give off a strong blue-green light, along with UV light. In order to further their commercialization, it was necessary to first correct the emission chromaticity by the use of luminescent materials, known as phosphors (Fig. 1). To achieve this, the blue-green emissions of mercury lamps were combined with red phosphors to achieve white light by means of exciting the red phosphors with the residual UV emissions from mercury.[19] Thus, the fluorescent lamp was born, consisting of a lamp made by combining a UV-emissive metal (typically mercury vapor), a noble gas (argon at first) to generate current through, and a visible-luminescent phosphor. The first versions were patented by Edmund Germer in 1927, who later licensed his invention to the General Electric Company.[20] The possibility to harness the UV emissions from gas discharge lamps and further convert them to visible emissions has kept these types of lamps in widespread use, even after the commercialization of more efficient technologies, like light-emitting diodes (LEDs). It is in the search for efficient and appropriate lighting that lanthanide-based phosphors became an important part of fluorescent lighting technologies.

Similarly, conversion to visible light is required when using a cathode-ray tube (CRT).[21] In a CRT, an electron gun generates a flow of charges, which can be deviated by the use of magnetic fields to hit a specific target on a screen. Such technology was mainly exploited in the production of televisions and instruments for the determination of wave behaviour, *e.g.* the oscilloscope. The conversion of the electron beam into luminescent signal on the screen must be achieved by the use of materials capable of generating charge carriers whose recombination provides luminescence, like in the LEDs described in Section 2.3. Lanthanide-based phosphors were particularly instrumental in bringing about CRT display technologies, especially in colour. Cathodoluminescence involves the transformation of electrons with high energy to light.[19]

Although the application of the phosphors in fluorescent lamps and CRT take advantage of different luminescence phenomena, the choice of the lanthanide phosphors is similar among all the different applications. The first commercial lanthanide-based phosphor was YVO_4:Eu^{3+}, introduced in 1965 by General Telephone & Electronics laboratories, for the purpose of using it in CRT-based colour television.[22] The 1960s have been referred to as the "golden age" of lanthanide phosphors, as most of the commercial ones were discovered during that time.[23] The production of lanthanide-based phosphors has not changed significantly over time, both because of the relative recency of their commercialization, and also because of the recent efforts to replace such phosphors with ones that are less affected by supply chain issues. When these technologies were proposed, lanthanides were still easily and reliably obtained.

The lanthanides played an undeniable role in producing CRT colour displays using a triphopshor system.[24] In this technology, the lanthanides brought about a high degree of colour purity, essential for producing realistic images. Briefly, in such an invention, a combination of three separate blue, green, and red phosphors are used in tandem to allow for a better colour rendering by taking into account the trichromatic perception of the human eye. The red-green-blue principle is still applied in the most recent display technologies.

Lanthanide phosphors can be made from a variety of different host materials.[21,25–29] The majority of blue light phosphors are based on the emissions from Eu^{2+} in several host materials, such as aluminates and chloroapatites. Green phosphors rely on the emissions from Tb^{3+} in oxysulfides and garnets, while red phosphors are commonly Eu^{3+}-doped oxides, phosphates, aluminates, oxi-chalcogenides, borates and sulfates. The phosphor set known as P22 was perhaps the most widely used tricolour set in commercial CRT monitors, where Y_2O_2S:Eu^{3+} represented the red component of the set.[30,31] In the decades since their introduction, CRT displays currently occupy a niche market, owing to the relative bulkiness of such devices. Notably, Thomas Electronics currently produces CRT displays and specify YAG:Tb^{3+}, better known as P53, as their default phosphor.[32] Since the eyes are well-adapted to detecting green light, monochromatic displays often use simple green phosphors for such a purpose. Most of their CRTs are developed for avionics and marine radar use.

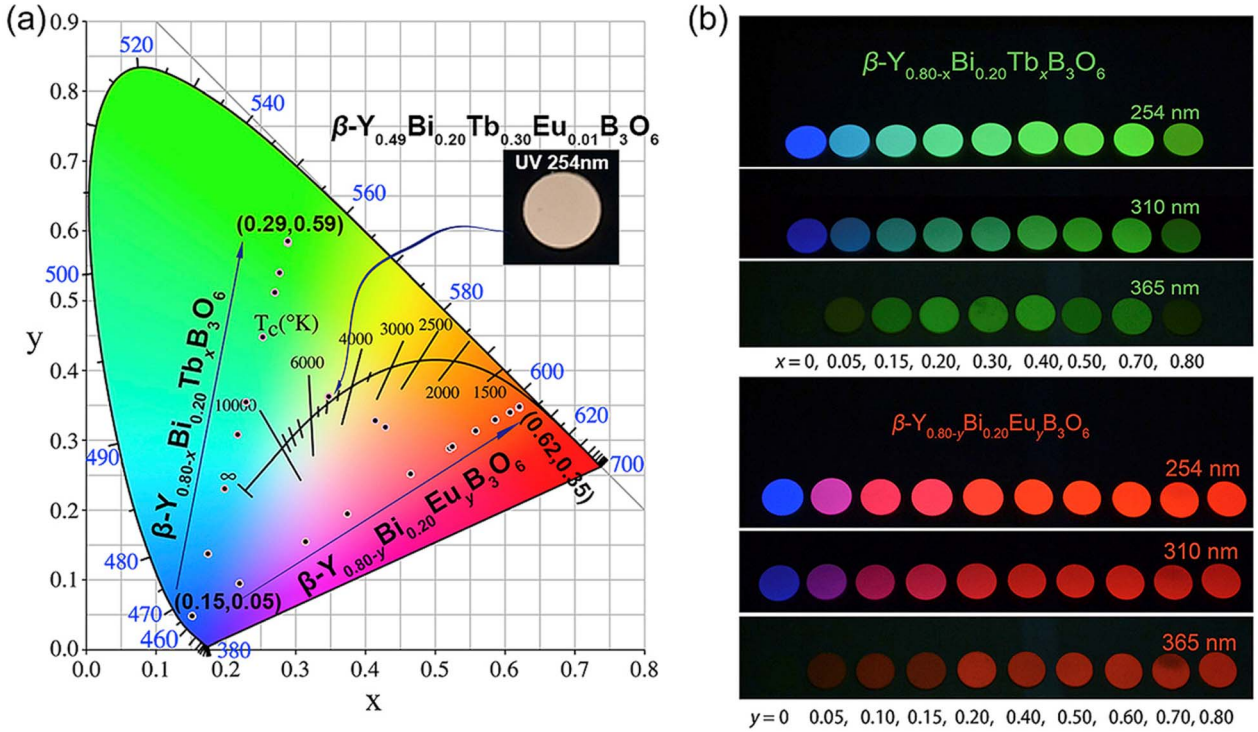

Fig. 1 (a) 1931 Commission Internationale de l'éclairage (CIE) diagram and corresponding positions of Eu^{3+} and Tb^{3+}-doped phosphors as a function of colour temperature and purity. The inset shows a white light phosphor under UV excitation at 254 nm. (b) The range of emission colours achieved by doping β-$YBiB_3O_6$ with different amounts of Tb^{3+} (top) and Eu^{3+} (bottom) under 254, 310 and 365 nm UV wavelengths. Reproduced with permission from ref. 29.

2.2 Lanthanides in light-emitting diodes (LEDs)

Light-emitting devices are all based on the principle of electrical pumping into semiconductor materials, with conversion of electric energy into luminescence.[33–35] Charge carriers can recombine as an excitonic emission, or *via* luminescent centers, which can be intrinsic to the semiconductor material or added as a dopant in the emissive layer; lanthanides have been used as dopants for this purpose.[34–36] The first blue LED was patented in 1973, based on GaN.[37] Today, the blue light from LEDs is mostly based on InGaN, which is in widespread use. This is what gives rise to the predominant blue emissions in modern colour displays. Rather than developing LEDs with intrinsic emissions of different colours, research has been devoted to finding ways to alter blue LEDs to emit other colours simultaneously, generating white light. The use of luminescent centers capable of such a conversion is the reason for the massive use of lanthanides in modern displays and LED lighting.

Lanthanides are used in LEDs either by doping the semiconductor active layer to transform its emission wavelength, or by coating the layers with lanthanide-based phosphors that are capable of absorbing the light emitted by the chosen LED and emitting a desirable visible wavelength.[34–36] The latter strategy was predominately used for the development of white light LEDs, which currently relies on lanthanide phosphors to achieve a range of white light colour temperatures.[38]

LEDs produced by direct doping of the semiconductors take advantage of the sharp emission lines of Eu^{3+} and Tb^{3+} to achieve colour purity, or the broadband emissions from Eu^{2+} and Ce^{3+} to obtain white emissions.[34–36] More commonly, phosphors are coated on top of the LEDs, avoiding direct contact with the active layer. In such a system, the phosphor simply re-absorbs the emitted light, which reduces the loss of the intrinsic emission from the semiconductor material. However, the spatial separation between the emitting semiconductor material and the lanthanide phosphor results in a lower absorption efficiency, dictated by the limited extinction coefficients of the lanthanide ions. If the two were in closer proximity, such limitations could be overcome by non-radiative energy transfer among the semiconductor and lanthanide ions, but it would change the semiconductor bandgap, leading to a less efficient intrinsic emission from the LED. Coating is consequently favored over co-doping.

Ce^{3+}-based phosphors present mainly green-yellow emissions, when singly-doped in aluminium garnets, aluminates, silicates and silico-nitrides.[39–41] Nitrides,[42] sulfides,[43] oxynitrides[44] singly doped with Eu^{2+} exhibit blue-green emissions depending on the chosen host. Ce^{3+} and Eu^{2+} co-doped silico-nitrides directly allow for the achievement of white light by combining blue light and these broadband emitters in multiple lumiphore layers.[64] The proposed structure allows for the interactions between successive layers, with the possibility to change the obtained colour chromaticity by varying the layer thicknesses.

The most efficient LEDs on the market are all based on lanthanide luminophores. Both Creed Inc and Philips reported LED efficiencies higher than 200 lm W^{-1} by the use of the very same technology described herein.[38] With respect to the common layering approach of different phosphors, Philips took a different approach to obtain its most efficient LED.[45] Using the light from InGaN, the blue emission is converted to green light by a luminophore containing Eu^{2+} and Ce^{3+}. Separately, a red LED is stacked, to achieve the final white emission with ultra-high intensity. The proposed architecture differs significantly from the others, which reported layering luminophores rather than alternating LED and luminophore layers. Such a successful case might move the industry in combining multiple point sources rather than using individual luminophores, which are still crucial for the LED industry.

With regard to displays, the Eu^{3+}-based red LEDs have become prominent. Even with the advent of liquid crystal displays (LCDs), incorporated lanthanide phosphors were still based on the same materials previously in development, with particular interest in vanadates and oxysulfides.[46] The further development of display technology is currently pointing towards organic materials, which results in the tendency to dismiss inorganic-based lumiphores for LED displays.

Despite these advancements, lanthanide luminescence is hindered by their intrinsic low absorption cross-sections. Current research is being carried out towards improving this by taking advantage of the antenna effect, through the use of ligands capable of absorbing the LED light and transferring it to the lanthanide luminescent center.[47,48]

2.3 Future perspectives on lighting and phosphors

Hybrid organic-LEDs (OLEDs) based on lanthanides are surely interesting materials for applications in lighting and displays.[49–51] The OLEDs have almost completely replaced LEDs, due to their higher performance in terms of resolution and colour rendering. Considering the strong electroluminescence efficiency of many lanthanide complexes, it seems counterintuitive that the OLED industries do not yet employ lanthanide-OLEDs in their current products on the market.[52–54] Likely, this is due to supply chain insecurities, though this may be remedied in the future as more lanthanide mining operations become active worldwide.[9] Regardless, lanthanides are uniquely able to achieve high colour purities due to their energy level structure, while obtaining high quantum efficiencies of the photon conversion process. These particularities are unique to the lanthanide series, which renders an auspicious future for the development of this sector.

3 Light amplification by the stimulated emission of radiation (LASER)

Trivalent lanthanides have constituted the luminescent center in the gain medium of many solid-state lasers. Introduced in 1962, the third laser produced was based on Nd^{3+} ions.[55] The development and applications of lasers, both on Earth and in space, are continuously booming, with a widespread involvement of the lanthanide ions in these technologies. The use of non-linear optics, different hosts, and activators produced a plethora of available laser technologies, with emissions ranging from the VUV to the NIR.[56,57]

Independently of the pumping source, whether electrical or photonic in nature, the functioning of a laser requires the excitation of the activator in the gain medium, which can either relax radiatively *via* spontaneous or stimulated emission.[57,58] Stimulated emissions require a photon of the pumping source to interact with photons in an excited state to obtain an emission, coherent with the pumping source. Both spontaneous and stimulated emissions can occur in an activator, and the probability of obtaining the required stimulated emission increases

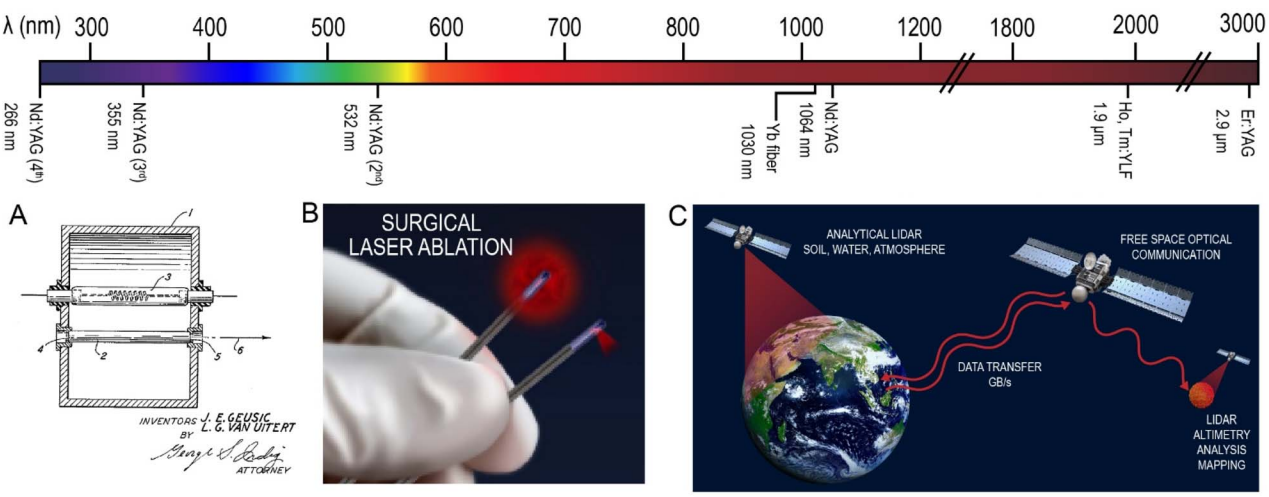

Fig. 2 (A) Original schematic of the Nd:YAG laser in the 1964 patent filed by Geusic and Van Uitert. (B) Photograph of the NeuroBlate® system by Monteris, which uses a Nd:YAG laser at 1064 nm for stereotactic laser ablation in neurosurgery. (C) Graphical depiction of the various ways infrared lasers are used in LIDAR and free space optical communication. Figures reprinted from ref. 55 and 82 with appropriate permissions.

with the lasing wavelength.[59] Thus, lanthanides with emissions in the NIR represent the most efficient activators for lasers, with Nd^{3+}-doped yttrium aluminum garnet (Nd:YAG) being one of the most commonly used lasers since its invention in 1964 by Joseph Geusic and LeGrand Van Uitert at Bell Telephone Laboratories.[60] As shown in Fig. 2, the Nd:YAG laser has a main emission at 1064 nm, but is also used in its frequency doubled, tripled and quadrupled forms at 532, 355 and 266 nm, respectively.

The advancements of laser technologies resulted in shortening of the pulse times to the femtosecond range. The superposition of the waves from the pumping laser and the activator emission during lasing determines the laser pulse width. A perfect superposition of the two waves corresponds to continuous conditions, while inversion of the population in a single shorter pulse can be obtained by allowing the build-up of the energy (Q-switching), by the interferences of multiple laser modes (mode locking), by external pumping with a shorter pulse width or by miniaturization of the laser cavity through the use of diodes or optical fibers.[61–63] These last two approaches are particularly interesting in view of the opportunity to release high power densities in an ultrafast time span. Nd:YAG lasers are still the most commonly encountered lasers in laboratories worldwide, particularly for their use in spectroscopy. Despite being one of the earliest lasers ever produced, the innovations discussed below promoted further applications than the simple spectroscopic analyses of luminescent materials. Shorter pulses can be achieved in Q-switching mode with the confinement of the cavity offered by the use of fibers or a pumping diode.

The obtained enhanced power and smaller size of the devices are particularly interesting with respect to one of the most common uses for lasers in industry: material ablation. With respect to large-scale ablation, the CO_2 lasers are most appropriate. However, the Nd^{3+} and Yb^{3+}-based lasers have recently received attentions in view of the possibility of using ultrafast lasers, which have been successfully applied to ablation in the micron and nano scale, applied in several industrial production sectors.[64–70]

3.1 Lasers in surgical procedures

Further opportunities in the medical surgical sector exploit the short pulses as a means of avoiding prolonged invasive treatments by the administration of high-power densities in short, single pulses. Laser ablation is one of the most important surgical advances, taking advantage of a variety of lasers ranging from the UV to NIR. Lasers for ophthalmic surgeries for cataracts were first patented in 1984, and relied on the emissions from nanosecond pulsed Nd:YAG lasers at 1064 nm.[71] Since then, femtosecond lasers based on Yb^{3+} have dominated the market for ophthalmic surgeries, as the faster pulses further minimize tissue damage, at a similar wavelength of 1030 nm.[72–75] Skin ablation for possible treatment of epithelial anomalies can also take advantage of Nd^{3+} and Er^{3+} NIR lasers at 1064 nm and 2.94 μm, respectively.[76–81] The laser irradiation can treat relatively deep tissues, by eliminating the problematic cells, such as in tumor removal (Fig. 2B).[82] The same medical approach can be applied to different body areas, as long as the penetration depth of the intervention allows the laser to reach it. Additionally, cosmetic surgeries also exploit laser treatments for ameliorating the appearance of bodily imperfections. Tattoo removal can be achieved through pulsed laser irradiating the area, showing particularly better results when the area is treated with shorter pulses. Notably, the different tattoo pigments are cleared by different laser wavelengths. In this respect, the frequency-doubled 532 nm emission from the Nd:YAG laser has been essential for removing red pigments, while the 1064 nm emission is used for blue and black pigment removal.[83,84] Cellulite, aging and scarring are other problems that these approaches are trying to improve, mostly by inducing minor damage to the skin to obtain a boosted production of collagen, which can help with each of these problems; Nd and Er:YAG lasers are primarily used for this purpose in a similar fashion to skin ablation discussed above.[85,86] Other aesthetic laser procedures are also available, such as aesthetic dentistry, ablation or hair laser removal.[87,88]

3.2 Free space optical communication

Free space optical (FSO) communication also exploits lanthanides for signaling within servers on Earth, or single and bidirectional communication from space. Wireless communications have enabled a global societal connection and facilitated space exploration. To achieve communication of information in free space, NIR laser diodes have been employed in the past, with the aim to transmit an optical signal among relatively close servers.[89] Although this technology has been replaced by fiber-coupled systems which guarantee a lower dissipation of the emitted light by amplification of the signal, as presented in Section 6, the reported example resulted in significant implications for achieving communication in space.

The advent of laser communication from space began from a simple experiment: the light from an argon laser sent from Earth was detected on the Moon.[90] Following this achievement, satellites and Earth bases were equipped with communication systems including lasers, which were devoted to wireless, free-space data transmission. Notably, the 1550 nm emission band from Er^{3+} is useful for optical communication between bases on earth, but is not ideal for communication to space due to meteorological intereferences.[91] With respect to deep space communication, however, the 1064 nm emission from Nd:YAG lasers have been used for communication between NASA terrestrial bases and spacecrafts orbiting Mercury and Mars.[92,93] Surprisingly for the time, the emission from the laser was detected at 24 000 000 km from the source, proving that lanthanide NIR lasers could be used for communication in deep space.[94] Bidirectional communication was first established using Nd^{3+}-doped lasers for communication, and signals were amplified using Er^{3+}-doped fibers at 1550 nm (see Section 6).[95,96]

Since these first missions, a plethora of satellites equipped with lasers have been sent to space. New challenges arose due to the need to move from near-Earth systems to technologies allowing deep-space communication, which requires high-power lasers designed to achieve long-distance

transmissions.[97–103] Moreover, the need for the transmission of large amounts of data resulted in the requirement for the lasing transmitting system to achieve a high signal rate. This requirement in part facilitated the creation of high-power and ultrafast laser facilities, like the Shanghai Superintense Ultrafast Laser Facility (SULF).[101,102] Similarly, scientists tried to enhance the data transmission rate, which achieved 319 TB s^{-1} as of 2021 between earth transmission bases.[104] Currently, the fastest commercial laser data transmission rates from space are in the GB s^{-1} range, still employing Nd:YAG lasers.[105,106] Only a few of the existing lanthanide-based lasers can fulfil the requirements in terms of power and rate of the signal for space communication, mostly based on previously proven technologies using the NIR emissions of Nd^{3+} and Yb^{3+} in diode and fiber lasers.

3.3 Light detection and ranging (LIDAR)

LIDAR takes advantage of laser coherence to determine the topology and/or composition of an environment by measuring the time-of-flight of the reflected signal.[89] Although the first laser to show promise for space communication was an argon laser, successive missions to determine the topology of planets like Mercury[94] and Mars[93] used lanthanide-based laser altimeters based on LIDAR. The possibility to miniaturize lasers and incorporate them into satellites permitted the opportunity to bring analytical spectroscopic equipment to space. It became possible to characterize the soil, water and atmospheric compositions of Earth and other celestial objects *via* interactions of the incident laser with matter through space LIDAR.[107–109] Most of the latest NASA missions using LIDAR employ lanthanide based-lasers, namely Ho^{3+} and Tm^{3+} co-doped $YLiF_4$ (Ho,Tm:YLF) or Nd:YAG.[109–114] This powerful tool became widely exploited in view of the possibility to monitor atmospheric parameters of the Earth such as pollutant concentrations, aerosol characteristics, wind analysis, and many others, all from space. This achievement provides a unique window for scientists to view the global situation in terms of greenhouse gas emissions and climate change. The pressing need to monitor the concentration of pollutants involved in the perturbation of the photochemistry of the atmosphere justified the necessity for space missions like the recent MERLIN (Methane Remote Sensing LIDAR Mission), which involved lanthanide lasers for methane detection.[114]

In summary, lanthanide-based lasers are ubiquitous, finding uses in a wide variety of industries. As technological advancements continue to be made, it is likely that they will continue to be produced and developed, finding new and potentially unexplored avenues for application.

4 Lanthanides in applications involving ionizing radiation

Radioluminescent materials emit light upon excitation with ionizing radiation. Scintillation is a type of radioluminescence characterized by fast luminescence decay times, on the order of hundreds of ns or shorter.[115] Scintillators have found widespread commercial use in detectors for medical imaging, homeland security, radiation safety and high energy physics experiments, among others. The desired properties of a scintillator are largely dependent on the intended application, as such it is well known that there is no single scintillating material that is universally optimal. The main luminescence properties that govern the choice of a scintillator are the emission wavelength, light output (photons emitted per MeV of energy absorbed), energy resolution, proportionality (linearity of emission with absorbed energy), and decay time.[116,117]

Lanthanide-based scintillator materials are among the highest-performing materials, with Ce^{3+}, Tb^{3+}, Pr^{3+} and $Eu^{2+/3+}$ in commercial use today (Fig. 3). The commercial success of these lanthanides is attributed to four main properties: their light yields, emission wavelengths, energy resolution, and decay times. Ce^{3+}-doped materials are used for their fast decay times, due to the allowed nature of the 5d → 4f transition of Ce^{3+}, which produces UV or visible light depending on the host material. Unlike the 4f → 4f transitions widely used for lanthanide luminescence, as described in the other sections of this review, the nature of the 5d → 4f transitions of the lanthanides is highly host dependent. For example, YAG:Ce^{3+} produces emissions at 532 nm, while $LaBr_3$:Ce^{3+} emits at 360 nm.[118,119] The position of the lowest 5d state relative to the conduction band shifts depending on the nature of the host, as described by the centroid shift and red shift models.[120] The position of the 5d state of Ce^{3+}, in turn, governs the emission wavelength of the 5d → 4f transition, and consequently the decay time, as the decay time is dependent on the third power of the emission wavelength of this transition.[121,122] The lifetimes of Ce^{3+} materials are among the fastest of the lanthanides, typically 100 ns or less, and can be as fast as 15 ns in the case of $LaBr_3$:Ce^{3+}, or as slow as 150 ns as in $Cs_2LiLaBr_6$:Ce^{3+} (CLLBC), which emits at 420 nm.[123,124] The 5d → 4f transitions of Pr^{3+} are actually faster (<20 ns) than Ce^{3+} in the same host due to the shift of the 5d levels relative to the conduction band previously

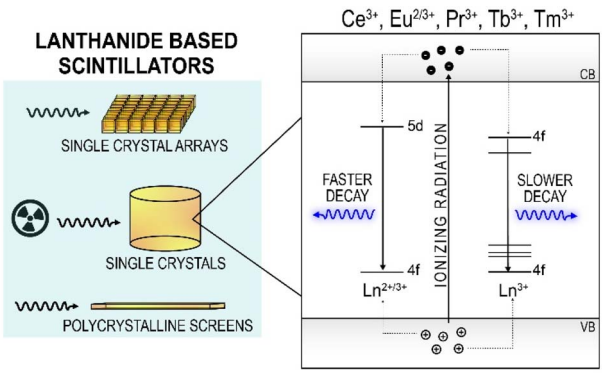

Fig. 3 Scintillators are commercially utilized in the form of crystalline arrays, single crystals, and polycrystalline screens. The most prominent lanthanide activators for such materials are Ce^{3+}, $Eu^{2+/3+}$, Pr^{3+}, Tb^{3+} and Tm^{3+}. The emissions from these activator ions can be classified by fast decay times (in the ns to ps range) for the allowed 5d → 4f transitions, or by slower decay times in the μs to ms range from the forbidden 4f → 4f transitions.

discussed.[117,122,125] The lowest 5d state of Pr^{3+} is 1.5 eV lower relative to the lowest 5d level of Ce^{3+} in the same host, explaining the faster lifetime.[120,125] Unfortunately, there are two main disadvantages of the d → f emissions from Pr^{3+} that have precluded their widespread commercial use. First, a lower light yield is typically obtained (two to three times lower than Ce^{3+} in the same host) due to de-excitation *via* a two-step process involving excitation of the $^3P_0$ state, which can also radiatively decay (these emissions are used in radiography, as discussed below).[117,126,127] Second, the interconfigurational emissions occur in the deep UV, which are not suitable for use with bialkali photomultiplier tubes (PMTs) and silicon detectors.[122,128,129] The $4f^6 5d \rightarrow 4f^7$ transition of Eu^{2+} is also an allowed transition, resulting in some of the highest light yields ever reported (120 000 photons per MeV for SrI_2:Eu^{2+}) and an emission wavelength of 435 nm. Despite the allowed nature of the 5d → 4f transition, Eu^{2+} compounds have relatively slow decay kinetics, around 1 μs, due to self-reabsorption.[117]

Afterglow, which is most generally defined as an additional, unwanted slow component to a decay time, is a major drawback to many materials and can severely limit their application.[130] While the primary decay time may be very fast, a secondary afterglow decay can cause imaging artifacts and limit detection speeds.[117,130,131] Afterglow is generally caused by the presence of trapping states that are introduced alongside defects in the crystalline material. In the case of materials that are intentionally doped with an activator ion (as is the case in most lanthanide-based scintillators), the introduction of these defects is unavoidable. In some cases, however, one can take advantage of the presence of trapping states, as has been done for X-ray storage phosphors, which have also contributed to medical imaging advancements, though they operate from very different mechanisms than scintillators (see Section 4.3.1).

The forbidden 4f → 4f transitions of Pr^{3+}, Eu^{3+}, Tb^{3+} and Tm^{3+} have achieved widespread commercial use in several medical imaging techniques, despite their relatively slow decay times (hundreds of μs to ms).[130,132,133] The $^3P_0 \rightarrow {}^3H_4$ transition of Pr^{3+} is a spin-allowed transition (centered at 514 nm in Gd_2O_2S:Pr^{3+} (GOS:Pr)) with a decay time of 3 μs, which is faster than any of the 4f → 4f transitions from Eu^{3+}, Tb^{3+} or Tm^{3+}.[133] Notably, despite the forbidden nature of this transition, it has a decay time that is close to that of the allowed interconfigurational transition of Eu^{2+}, illustrating just how fast of a decay time this is for a 4f → 4f transition. The red emission from Eu^{3+} at 610 nm from the $^5D_0 \rightarrow {}^7F_2$ transition is well suited to silicon detectors, but it has a decay time on the order of ms.[134] Tb^{3+} has predominately green emissions that are maximized at 545 nm from the $^5D_4 \rightarrow {}^7F_5$ transition, which also has decay times on the order of ms.[135] The long decay times of Eu^{3+} and Tb^{3+} preclude their use from most applications of scintillators, though they have played an important role in advancing medical imaging, as will be discussed later.

Traditionally, single crystal scintillators are most often used. Because of this, a major factor in the success of commercial scintillator compositions is the ease, time and cost of growing high-quality single crystals.[117,136,137] More recently, polycrystalline powders and crystalline fibers have become more widespread as they are easier to synthesize and provide more flexibility in the shape and geometry of the detector, as well as the ability to generate small pixel arrays.[117,136]

4.1 National security

Scintillators are essential components of radiation detectors manufactured for use in radiation monitoring, special nuclear weapons detection and radioisotope identification, weapons detection, illegal cargo detection, and other security fields.[122,135,138] Lanthanide-based scintillators are primarily used in these fields for gamma ray spectroscopy, X-ray imaging and computed tomography. In all of these cases, it is essential that detection can be achieved rapidly and with high sensitivity to ensure high-throughput inspection at airports and border crossings, and to be able to detect small quantities of contraband. In these applications, high light yields, high proportionality and minimal afterglow are desired.

4.1.1 Imaging-based inspection. Much like clinical X-ray imaging, luggage and cargo inspection imaging has similar requirements, but on a much larger scale. Thus, large-screen flat panel displays made of polycrystalline ceramics like GOS:Tb^{3+} are more cost effective and feasible than producing large single crystal detector arrays.[139] For industrial X-ray imaging, systems from LINEV ADANI and Teledyne DALSA used in vehicle, cargo, luggage and full-body scanning employ CsI:Tl^{3+} or GOS:Tb^{3+} as the scintillator component for high energy X-ray imaging.[135,140] Since high-throughput inspection is of paramount importance in screening of large amounts of cargo in a short period of time, a lack of afterglow combined with a high light yield are considered essential to provide good contrast.[135,136,138] Thus GOS:Tb^{3+}(Eu^{2+}) is widely used and preferred in this respect, with a light yield of 60 000 photons/MeV and no afterglow component.[122,135] Of course, the price of lanthanide-based detectors is higher, which can become a prohibitive factor for the large detector arrays needed for vehicle inspection, for example. In cases where lower resolution can be tolerated, Tl^{3+}-based scintillators provide a cheaper alternative.

Computed tomography is also used to inspect cargo, vehicle and luggage, since it allows for the imaging of low atomic number materials such as textiles and plastics in addition to high atomic number metallic components. The technological requirements for non-medical CT-based detectors are similar to what is needed in the medical imaging field, but the detectors need to be larger to accommodate vehicles and cargo containers, for example. Notably, complementary metal oxide semiconductor (CMOS)-based detectors are now being offered as an alternative to bialkali PMT and amorphous silicon detectors, and are sensitive to the green emissions from Tb^{3+}.[140] GOS:Tb^{3+} screens have low afterglow and can be used repeatedly. Thus, when coupled to a CMOS sensor, they allow for high frame-rate digital X-ray imaging with good spatial resolution.[140] The Rad-icon product family from Teledyne DALSA advertise their CMOS/GOS:Tb^{3+} based detectors for use in large-scale computed tomography.[141] The high frame rates make it possible to inspect large quantities of cargo in a drive-through manner, for example.

4.1.2 Radiation detection and identification. Radiation and radioisotope identification and detection (RIID) also relies on the use of scintillator crystals. Energy resolution is a measure of the ability of a scintillator to distinguish between gamma rays of slightly different energy and is dependent on the light yield and proportionality (expected # photons emitted as a function of energy absorbed) of the scintillator material. These properties are essential in gamma spectroscopy to rapidly and accurately identify gamma signatures of radioactive materials, such as those of weapons-grade plutonium, enriched uranium, or mixtures of materials.[122,138,142] Ce^{3+}-doped crystals like $LaBr_3$:Ce^{3+} and $CeBr_3$ are among the most widely used scintillators for this purpose and exhibit high light yields (60 000 photons per MeV or higher), fast decay times (<20 ns), and detect gamma rays with high energy resolution at 662 keV (<3%).[121,122,135] Interestingly, lanthanum has its own characteristic radioactivity, which results in a higher background signal. Since one of the main techniques in gamma spectroscopy is pulse height discrimination, intrinsic radioactivity can make it more difficult to differentiate between peaks. Thus, $CeBr_3$ was developed as a background-free alternative and is licensed to Hellma Materials for commercial production. Both $LaBr_3$:Ce^{3+} and $CeBr_3$ are used in commercial radiation isotope identification devices manufactured by Berkeley Nucleonics Corp.[143] Ce^{3+}-activated ^{6}Li-doped glasses and elpasolite crystals have made it possible to combine gamma and thermal neutron detection into a single component. This became essential after the rapid onset shortage of ^{3}He in 2008, as ^{3}He was the gold-standard in thermal neutron detectors at the time.[138] Pulse-shape discrimination is used to differentiate between neutrons and gamma sources using scintillation from Ce^{3+}. Ce^{3+}-doped elpasolite crystals have higher light yields than their glass counterparts and are better suited for smaller devices.[144] The first commercially-available personal RIID detectors for gamma and neutron detection *via* a single material are based on CLYC (Cs_2LiYCl_6:Ce^{3+}) and were produced in 2014 by ThermoScientific (RadEye+).[145] Shortly thereafter, around 2017, companies like Saint-Gobain Crystals, CapeScint, Berkeley Nucleonics and RMD began commercially producing and using CLLBC, which has a substantially higher light yield than CLYC.[124,146] Even more recently, SrI_2:Eu^{2+} has been rediscovered as an option for use in radiation detection, owing to its extremely high light yield (100 000 photons per MeV, near its theoretical limit), blue emission at 435 nm that is well-suited to detection by silicon photomultiplier (SiPM) detectors, and extremely high energy resolution (2.6% at 662 keV).[117,122] The main drawback to the widespread use of SrI_2:Eu^{2+} is its relatively slow decay time, which is an order of magnitude slower than Ce^{3+}. SrI_2:Eu^{2+} was first investigated for commercial use in the 1950s, but failed due to inadequate crystal growth techniques.[117,122] Today, synthetic technologies have advanced, and CapeScint produces detectors such as the RadSolver™ RIID using SrI_2:Eu^{2+}. It is expected that Eu^{2+}-based halide detectors like this will reach widespread use alongside their Ce^{3+} counterparts.[117,136,147,148]

4.2 Scintillators for well-logging

The oil and natural gas industries use gamma and neutron detection methods in well-logging to identify potential reservoirs.[149] In this case, scintillators for gamma spectroscopy with neutron detection capability are essential, but the scintillators must also be compact and rugged to account for the harsh vibrations and temperatures experienced in the small boreholes used in logging.[150] For this reason, crystalline materials that are prone to cracking or have luminescence that is strongly temperature dependent cannot be used. Thus, options that are useful for gamma spectroscopy in personal dosimeters or stationary radiation monitoring systems may be eliminated simply due to the environmental factors that affect performance. In the 1980's, NaI(Tl) was the main option for logging in boreholes,[150] but today, this is no longer the case, and lanthanide-based scintillators, such as $LaBr_3$:Ce^{3+} and $Gd_{1.8}Y_{0.2}SiO$:Ce^{3+}, are commonly employed.[151] The well-logging industry also needed to transition from ^{3}He neutron detectors, thus ^{6}Li-based materials doped with Ce^{3+} and Eu^{3+} became more common. Schlumberger Technology Corp currently holds a patent[152] on LiCAF:Eu^{3+} for neutron detection in oilfield applications, solidifying the idea that Eu^{3+} based scintillators like SrI_2:Eu^{3+} are strong alternatives for Ce^{3+} based materials. A US patent on the methods for neutron imaging in boreholes based on scintillation detectors was published in December 2022, suggesting lanthanide-based scintillator technologies are a fundamental aspect of advancing the technologies used in the oil industry.[153]

4.3 Medical imaging

4.3.1 X-ray radiography. Widespread clinical use of X-ray radiography was achieved using a film/screen system, which was used for decades. In the mid-1970s, the development of lanthanide-based intensifying screens made from GOS:Tb^{3+} and LaOBr:Tm^{3+} made it possible to significantly reduce the radiation doses necessary to produce an image using standard $CaWO_4$ screens, which have a lower X-ray absorption cross-section and a lower light yield.[154,155] In fact, lanthanide-based imaging screens allowed for a reduction in radiation exposure by 60–70% for a variety of different anatomical regions, with minimal differences in image quality, due to their high photon conversion efficiencies.[155] The green and blue emissions from Tb^{3+} and Tm^{3+}, respectively, were well-suited to generating images on film, which is most sensitive to the blue-green spectral region. However, in the 1980s, a transition from film-screen radiography to digital imaging was inevitable.

Lanthanide-based X-ray storage phosphors were instrumental in the transition to digital X-ray radiography. The development of computed radiography (CR) based on the use of BaFX:Eu^{2+} (X = Cl^-, Br^-) imaging plates allowed for this transition.[156] Unlike scintillator-based imaging, where emitted light is immediately detected and used to generate an image, X-ray storage phosphors absorb energy and convert it to metastable trapped charge, which can then be released at a later timepoint for processing. In this way, a storage phosphor screen stores a latent image and can be erased and reused hundreds of

times.[156,157] In the case of BaFX:Eu^{2+} (X = Cl^-,Br^-), after X-ray exposure, trapped charge can be released *via* excitation with red light to produce an emission from Eu^{2+} at 390 nm, with a decay time of 800 ns.[132] Practically, the readout is done using a laser that scans the phosphor screen to visualize the latent image. The emission band from the allowed 5d–4f transition of Eu^{2+} overlaps well with the most efficient regions of bialkali PMTs, and the fast decay time allows for rapid scanning to generate the digital image quickly.[157] Moreover, the fast decay time is essential for preventing imaging artifacts. The first CR imaging plates were produced by Fuji in the 1980s, and Eu^{2+}-based plates were the mainstay of radiography for about a decade thereafter.[132,156] Notably, phosphors based on Eu^{2+} such as BaFX:Eu^{2+} (X = Cl^-,Br^-) and CsBr:Eu^{2+} are still at the forefront of CR-based imaging technologies. Today, needle-image plates composed of CsBr:Eu^{2+} provide images at comparable or higher qualities and lower radiation doses than what can be achieved using CsI:Tl^+ plates that came into use when digital radiography techniques were invented.[157,158] CsBr:Eu^{2+} is a particularly interesting material because it can be grown into small needles in the same way as CsI:Tl^+; this is the property that allows CsI(Tl) to provide higher resolution than BaFX:Eu^{2+} (X = Cl^-,Br^-). As such, it may be a strong competitor for the market that CsI(Tl) occupies. Today, Fuji, Carestream and Agfa are the main companies actively involved in R&D of storage phosphors for improved CR imaging technologies.[156]

The multistep process of acquiring a latent image and then reading it out using a separate device was a major motivator for the development of flat-panel digital radiography. First introduced in the mid-1990s, flat panel imaging is based on the incorporation of a semiconductor detector that can either directly convert X-ray radiation to electrical signal, or do so through an intermediate scintillator layer in an indirect fashion.[156] While direct imaging may seem like the obvious choice, the amorphous selenium detectors used for X-ray detection have lower density and atomic number than most scintillators. Thus, they have lower radiation stopping powers and therefore must be thicker relative to the indirect counterparts. For indirect imaging, scintillators like GOS:Tb^{3+} are ideal for reasons similar to their use in intensifying screens for screen-film radiography. Notably, CsI(Tl) is the only non-lanthanide material that is in widespread commercial use for X-ray radiography. Relative to GOS:Tb^{3+}, CsI(Tl) scintillators are slightly hygroscopic and a significant afterglow component limits imaging acquisition speeds, reduces spatial resolution and introduces artifacts.[117,122] As such, both materials have their advantages and disadvantages, as is the case for all scintillator materials.

4.3.2 Computed tomography. Computed tomography (CT) is an X-ray imaging technique that produces high resolution images of both soft tissues and bones, unlike in conventional X-ray imaging. This is achieved by positioning the X-ray source and the detector across from one another and rotating them in tandem around the patient to achieve a 360° scan. To achieve rapid scan times, produce images with high signal-to-noise ratios, good spatial resolution, and minimize the radiation dose to patients, the optimal scintillator materials must have high X-ray stopping powers in the keV range (and therefore a high density), high light yields, minimal afterglow and high radiation resistance. $CdWO_4$ was the standard single crystal scintillator used for CT detectors because of its high density and good optical transparency.[122] However, it has a significant afterglow component, it is known to accumulate radiation damage, and the toxicity of cadmium poses a threat during manufacturing and waste disposal.[130] Moreover, single crystals are difficult and expensive to grow with high uniformity, which is important for minimizing imaging artifacts due to detector inhomogeneities. For these reasons, lanthanide-based polycrystalline ceramic scintillators have become widely used in CT detectors.[122] Specifically, GE Medical System's HiLight™ $(Y,Gd)_2O_3:Eu^{3+}$ scintillator was introduced in their Optima CT scanners starting in 1988,[134] $Gd_2O_2S:Pr^{3+}$ was introduced by Siemens under the brand name UFC™ (ultra fast ceramics) in their commercial clinical SOMATOM Definition CT scanners in the late 90s/early 2000s,[159,160] and $Gd_2O_2S:Pr^{3+}$, Ce^{3+}, F^- was introduced by Hitachi Metals in the late 1990s.[130,133,161] In the Pr^{3+}-emitting ceramics, emission maxima are obtained at 513 nm from the $^3P_0 \rightarrow {}^3H_4$ transition, as previously mentioned, it has a relatively fast decay time of 3 μs. The detected red emissions from Eu^{3+} arise from the $^5D_0 \rightarrow {}^7F_J$ transitions, which have a considerably longer decay time (960 μs).[134] The red emissions from Eu^{3+} are more convenient for detection by silicon photodiodes than the green emissions of Pr^{3+}. However, the decay time of the scintillator restricts the imaging rotation speed, thus the fast decay times of Pr^{3+} are preferrable in that respect. High X-ray attenuation coefficients are essential for complete attenuation of incoming X-ray photons to prevent damage to the Si photodiodes that are coupled to the scintillators and convert light intensity into a current signal. With respect to attenuation, HiLight™ requires twice the thickness of UFC™ to stop the same percentage of X-ray photons. However, the hexagonal crystal structure of GOS results in a translucent crystal due to light scattering, while HiLight™ is entirely transparent. In that respect, a greater number of photons can reach the detector from the transparent crystal. Thus, there are advantages and disadvantages to both ceramic materials, and each has allowed for tremendous advancement in CT imaging in their own right. The use of these lanthanide-based polycrystalline scintillators has allowed for thinner detector panels with more uniform pixels, faster scanning speeds and higher signal to noise ratios, both of which have led to higher spatial resolution and a reduction in radiation dose to patients. More recently, GE Healthcare has introduced the GE Gemstone™, which is a lanthanide-based garnet scintillator that has been incorporated into dual-source CT scanners, where X-ray sources of high and low energy are alternated during a single imaging rotation to achieve improved anatomical contrast using temporal resolution. The GE Gemstone™ boasts a decay time of 30 ns, which is considerably faster than the decay time of Pr^{3+}, and with lower afterglow (Fig. 4A).[159] Presumably, the GE Gemstone™ is based on Ce^{3+}, as companies like C&A Japan have made press releases about the manufacturing of GAGG:Ce^{3+} arrays,[162] and others have described the promise of other Ce^{3+} garnets such as

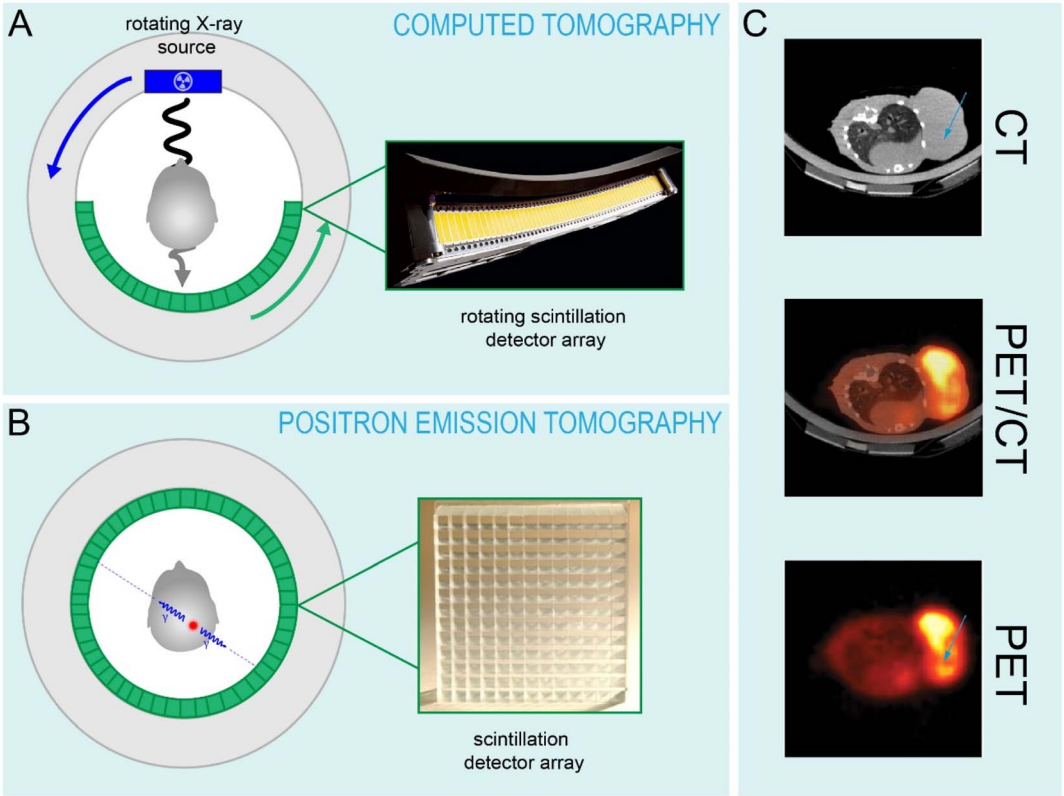

Fig. 4 (A) Schematic of the principle of a computed tomography (CT) scanner. The rotating scintillation detector array shown is a GE Gemstone array. Detector photograph courtesy of GE. (B) Schematic of a positron emission tomography (PET) scanner. The scintillation detector array shown is a 13 × 13 LSO:Ce^{3+} array. Each scintillator crystal is 4 mm in diameter. (C) CT (top), PET (bottom) and combined PET/CT (middle) images of a mouse bearing a tumor. GE array. LSO detector array photographs and mouse imaging photographs modified from ref. 157.

LuAG:Ce^{3+} for this application.[118,136] These materials have also paved the way for combined PET/CT detectors, as discussed below.

4.3.3 PET imaging. Positron emission tomography (PET) imaging relies on the simultaneous position-sensitive detection of two gamma rays to form a line of detection which can be traced back to a location inside a patient's body (Fig. 4B). The need to correlate the detection of photons in time and space therefore requires fast decay times and high light yields to achieve rapid signalling with minimal event accumulation, but also high density to attenuate gamma photons. For decades, PET scanners employed BGO as the scintillator detector component, but the relatively low light yield (9000 photons per MeV) and decay time (300 ns) limited further improvements to this imaging technique.[163] This prompted the development of Lu_2SiO_5:Ce^{3+} (LSO), which has a much higher light yield (26 000 photons per MeV) and faster decay time (40 ns) than BGO. Similar crystals such as Gd_2SiO_5:Ce^{3+} (GSO) were also developed, but GSO has a significantly lower light yield (7600 photons per MeV) with a comparable decay time (60 ns). In the late 1990s, the first PET scanners employing LSO:Ce^{3+} (ECAT ACCEL, Siemens) and GSO:Ce^{3+} (Allegro, Philips Healthcare) were produced.[130,164] Yet again, the allowed 5d → 4f transitions of Ce^{3+} that give rise to fast decay times facilitated important technological advancements. Specifically, the high light yield from Ce^{3+} in LSO allows for better spatial resolution, and the fast decay times of Ce^{3+} in LSO and in LYSO (containing a portion of Y^{3+} in place of Lu^{3+}) have enabled time-of-flight (TOF) PET imaging, as the 40 ns decay times make it possible to correlate positron annihilation events with high temporal precision.[119,165,166] Specialized PET scanners for positron emission mammography (PEM) are also made and rely on the use of these LYSO:Ce^{3+}. The only commercially available PEM scanner, the NaviScan Flex Solo II™, utilizes LYSO:Ce^{3+} because it is imperative that minimal radiation doses are delivered to breast tissue during scanning, thus extremely fast imaging capabilities are required.[167,168]

For nearly a decade, no single-modality PET scanners have been produced.[164] Rather, there has been a transition to combined PET/CT imaging within a single gantry, as the anatomical information provided by CT provides greater information about the location of malignancies that are detected by PET (Fig. 4C). Unfortunately, the properties that make a scintillator favorable for use in PET or CT are not mutual, so a scintillator detector panel that can do both imaging modalities has not been yet achieved. The significant afterglow component in LSO:Ce^{3+} precludes its use as a CT detector, while the relatively slow decay times of Eu^{3+} and Pr^{3+} preclude their use in PET.[169] Current generation TOF-PET/CT scanners like the Siemens BiographVision™ and Philips Gemini™ TF scanners

employ LSO:Ce^{3+} and LYSO:Ce^{3+}, respectively, for PET and GOS:Pr^{3+} (UFC™) for CT. State of the art clinically used TOF-PET/CT devices all employ lanthanide-based scintillators in one or both detector components, and are able to achieve temporal resolutions down to hundreds of picoseconds, which has enabled higher signal to noise and better spatial resolution, as well as quantitative dosimetry for radiotherapy treatment planning.[131,164,169–171] Interestingly, GE announced in October 2022 a new generation of PET/CT scanners (Omni Legend) that utilize BGO crystals for the PET component, which is essentially full-circle in the PET detection field.[172] In this case, it is not the efficiency of the scintillator, but the efficiency of the other detector components that enables the use of a lower light yield, slower scintillator crystal. Even in the case of the BiographVision™ 600, which uses LSO:Ce^{3+}, the introduction of a SiPM detector array instead of PMTs enabled tremendous advancements in terms of scintillator-detector overlap and signal acquisition.[171] Notably, the search for scintillators that can continue to advance these imaging modalities is at the forefront of the materials science field.[131] However, the advancements that will be generated are likely to be in finding hosts that enable higher attenuation, higher light yields, better energy resolution and higher optical transparency, and that can be produced at high qualities at low cost. Combined, these advancements would enable lanthanide luminescence to be harnessed at maximum efficiency by the next generation of medical imaging detectors.

4.4 Electron microscopy

Electron microscopy also relies on the use of scintillator-based imaging and benefits from the same advancements made in medical imaging. In electron microscopy, it is often necessary to use rapid acquisition times, as samples can often degrade under the electron beam. Moreover, the image can be degraded by scattering if the phosphor screen used for viewing is too thick. For these reasons, scintillators with high light yields, high densities, fast decay times and minimal afterglow are desired. Early electron microscopy relied on visual inspection of the generated image, and green phosphors were desired owing to the sensitivity of the eye in the green spectral region.[173] Tb^{3+} based phosphors became routinely used in the viewing screens for electron microscopy alongside other green phosphors such as ZnS:Cu. Today, GOS:Tb^{3+} is still commercially available for use in viewing screens, usually marketed under the common name P43.[174] However, the long decay time of Tb^{3+} (1 ms) motivated researchers to use YAG:Ce^{3+}, known as P46, which has an emission maximum at 530 nm and a decay time of 300 ns, with a much shorter afterglow component than GOS:Tb^{3+}. When Tb^{3+} is added to P46, the P47 phosphor was developed, which has a blue emission but an even faster decay time at 100 ns.[174] While the Ce^{3+}-based viewing screens have much faster decay times, GOS:Tb^{3+} has a higher light yield, which allows for more sensitive detection. The first all-digital microscopes were also made possible by lanthanide scintillators, and employed YAG:Ce^{3+} coupled to fiber optics and bonded to CCD or CMOS detectors to generate images.[175] In contrast to microcrystalline viewing screens for the detection of primary electrons, back-scattered electrons (BSE) and secondary electron detection require the use of single crystals. The small number of electrons detected by the annular detectors at high and low scattering angles make single crystal detectors the best option for providing the highest quality images with good contrast.[176] Ce^{3+} garnet (YAP:Ce^{3+} and YAG:Ce^{3+}) single crystals are employed in the REBEKA™ and KARMEN™ scanning electron microscope BSE detectors made by CRYTUR Ltd.[177,178] In 2021, Gatan Inc. was granted a patent on microcrystalline Ce^{3+} and Pr^{3+} garnets for use in electron microscopy, suggesting there will be new imaging technologies based on scintillators with much faster decay times.[179] As direct electron detectors become more commonplace, lanthanide-based technologies may likely remain as an alternative option.

4.5 Astronomy

Scintillators also play an important role in astronomy, especially given that the cost-benefit consideration is far different from that in industry, as mentioned in the introduction. Highly specialized detectors are needed and are often custom designed for a specific application, mostly for various gamma and X-ray spectroscopy studies. Gamma ray spectroscopy is used in interplanetary space missions to study terrestrial and atmospheric compositions of planets, solar flares, and extra-galactic bodies such as black holes, stars and supernovas. X-ray spectroscopy is also used for those purposes, along with studies of hot gasses and objects falling into black holes. For both X-rays and gamma rays, it may be desirable to produce images, spectra to detect elemental signatures, or time-of-flight data to ascertain the location of a radiation source.[180] Each of these goals requires scintillators with different properties, and most of them need to have fast decay times, high light yields and be of sufficiently high density to attenuate MeV and GeV photons. Especially with respect to extragalactic bodies, low photon fluxes from these distant sources mean highly sensitive detectors are a necessity. With respect to density, this can often mean the thickness of the scintillator (and consequently the weight) are of concern, as there is generally a desire to have instruments as compact as possible. NASA missions are currently using probes employing Ce^{3+}-based scintillators like CLYC and CLLB (Glowbug[181]) and SrI_2:Eu^{3+} (Strontium Iodide Radiation Instrumentation II (SIRI-2)[182]) for gamma-ray spectroscopy. The Gamma Ray Neutron Spectrometer (GRNS) aboard the Messenger Spacecraft that orbited Mercury for several years employed a Ce^{3+}-doped ^{6}Li glass to detect both gamma rays and neutrons in a similar manner as the Glowbug detector. The European Space Agency used GOS:Tb^{3+} supplied by Scintacor in the PROBA2 detector to image the solar corona *via* detection of high-energy UV photons.[183,184] This is one of the few examples found where polycrystalline materials were used. Compton cameras/telescopes are also used to detect gamma rays but rely on the kinematics of Compton scattering to generate images. $CeBr_3$ is used in NASA's Advanced Scintillator Compton Telescope (ASCOT),[185] and $LaBr_3$ was used for time of flight measurements of the FAst Compton TELescope (FACTEL).[186]

ASCOT is a successor to a previous mission called COMPTEL, which used NaI(Tl). The ASCOT $CeBr_3$ had a time-of-flight resolution of 225 ps, while COMPTEL had a resolution of 1 ns, thus the use of $CeBr_3$ provided a nearly four-fold improvement in resolution over its NaI(Tl)-based predecessor.[180,185] Notably, the rest of the design was the same as the COMPTEL instrument and only the scintillator was changed. The Japanese Space Agency JAXA and NASA collaborated on the Astro E2 "Suzaku" satellite, upon which GSO:Ce^{3+} detectors were used in the hard X-ray detector, HXD-II, until 2015 when the satellite was decommissioned.[187,188] The GSO:Ce^{3+} detectors were manufactured by Hitachi Chemical Co. and achieved energy resolutions better than that of the IBIS spectrometer aboard the ESA's INTEGRAL spacecraft, which used CsI detectors.[188,189] Launched in 2017, the China Seismo Electromagnetic Satellite (CSES) is a collaboration between the Italian Space Agency and the Chinese Manned Space Agency that is monitoring the stability of the Van Allen radiation belts using LYSO:Ce^{3+}-based detectors.[190,191] LYSO:Ce^{3+} was chosen for its good energy resolution and ability to fully attenuate protons and electrons that are up to 250 MeV in energy. In most cases, lanthanide-based scintillators outperform the traditional BGO, CsI(Tl) and NaI(Tl) scintillators, and are the preferred materials when extremely high performance is desired and cost is not the prohibitive obstacle. The continued development of technologies used for astronomy experiments will almost certainly benefit from advancements made in materials science as well.

5 Anti-counterfeiting

Recent estimates have suggested that approximately $500 billion USD of counterfeit or pirated goods are sold each year, accounting for over 2% of global trade.[192] This number is only expected to rise with the increase in popularity of e-commerce and online shopping, making it more difficult to verify the validity of goods or products. The most prevalent industries affected by counterfeit goods include footwear and textiles, jewelry, electrical and medical equipment, and even pharmaceuticals.[193] As a result, the distribution of counterfeit products not only impacts the economy but also has health implications, especially in developing nations, due to counterfeit antibiotics or other medication distributed in low-income countries.[194] Therefore, industry manufacturers look to tag or label their products with characteristic and unique markers that distinguish them from counterfeits.

Known as taggants, the unique labels that manufacturers rely on to identify their goods can assume many forms, including physical, chemical, or spectroscopic markers.[195,196] The benefit of spectroscopic markers is that they're non-destructive, invisible, and highly versatile, due to the wide variety of possible excitation and emission wavelengths. They can either be fluorescent molecules or inorganic phosphors, although, some uncertainties in the chemical and photostability exist for the organic molecular taggants.[197] Thus, many companies, contracted by industry to secure their goods, utilize phosphors as spectroscopic taggants. These phosphors often contain lanthanide ions, such as europium or cerium, due to their robust, characteristic, and bright emission spectra.

There are documented instances of lanthanide-doped phosphors used in anti-counterfeiting, though this list remains limited since agencies do not advertise the exact nature of their taggants. Companies that explicitly promote the use of lanthanides as the basis of their phosphors are therefore scarce. Among them, the HelioSUITE from Luminescence Sun Chemical Security advertises luminescent inks that can improve the security of banknotes and other government documents.[198] Honeywell's Lumilux® exploits inorganic phosphors that can be embedded into plastic cases, fabrics or metals to help secure a variety of goods.[199] This technology aims at markets that include healthcare, food products, as well as the automotive industry. Similarly, Olnica advertises rare-earth compounds that can be inserted in plastics and paper to make secure food packaging and security labels.[200]

Evidently, counterfeiting extends beyond private corporations, as government documents are also subject to forgery and imitation.[201,202] Therefore, countries are required to invest heavily in security measures that prevent fraudulent documentation, and every nation does so differently. Some countries use lanthanide-doped phosphors as spectroscopic taggants embedded in banknotes and other documents. Under ultraviolet excitation, these luminescent features are observed on different currencies and passports from around the world, as presented in Fig. 5. While the exact identity of the different phosphors is intentionally unknown, speculating on their composition acts as a good exercise to showcase the practicality of incorporating lanthanide-doped phosphors to prevent counterfeiting.

The first anti-counterfeiting feature shown in each of the banknotes photographed in Fig. 5, under UV irradiation, is the presence of some luminescent dashes and speckles. A known technique in anti-counterfeiting is the physical unclonable function (PUF), in which a patterned tag is generated through a stochastic process and recorded ahead of distribution.[203] By definition, each pattern is unique and non-reproducible. A recorded image is stored by the manufacturer and only shared with parties that need this key for authentication purposes. Regardless of the emission color, one feature on all banknotes that use spectroscopic taggants is a speckle pattern that is comprised of one or more phosphors, generating a PUF. In some instances, such as the euro, the fibers even alternate colors, forming a more complex feature. These luminescent fibers are randomly distributed across the entire banknote, making each one unique. If the banknotes are irradiated with ultraviolet light and photographed ahead of circulation, banks can cross-reference each note using its serial number to ensure its authenticity. By using multiple phosphors, the encryption can be made even more complex.[204] One such limitation to this technique is the resolution of the stored photographs, where the number of photographed pixels increases the encoding capacity exponentially.

A second evident anti-counterfeiting measure is based on the uniqueness of the characteristic emission spectra of the chosen phosphors, as shown in the emission spectra of Fig. 5. For

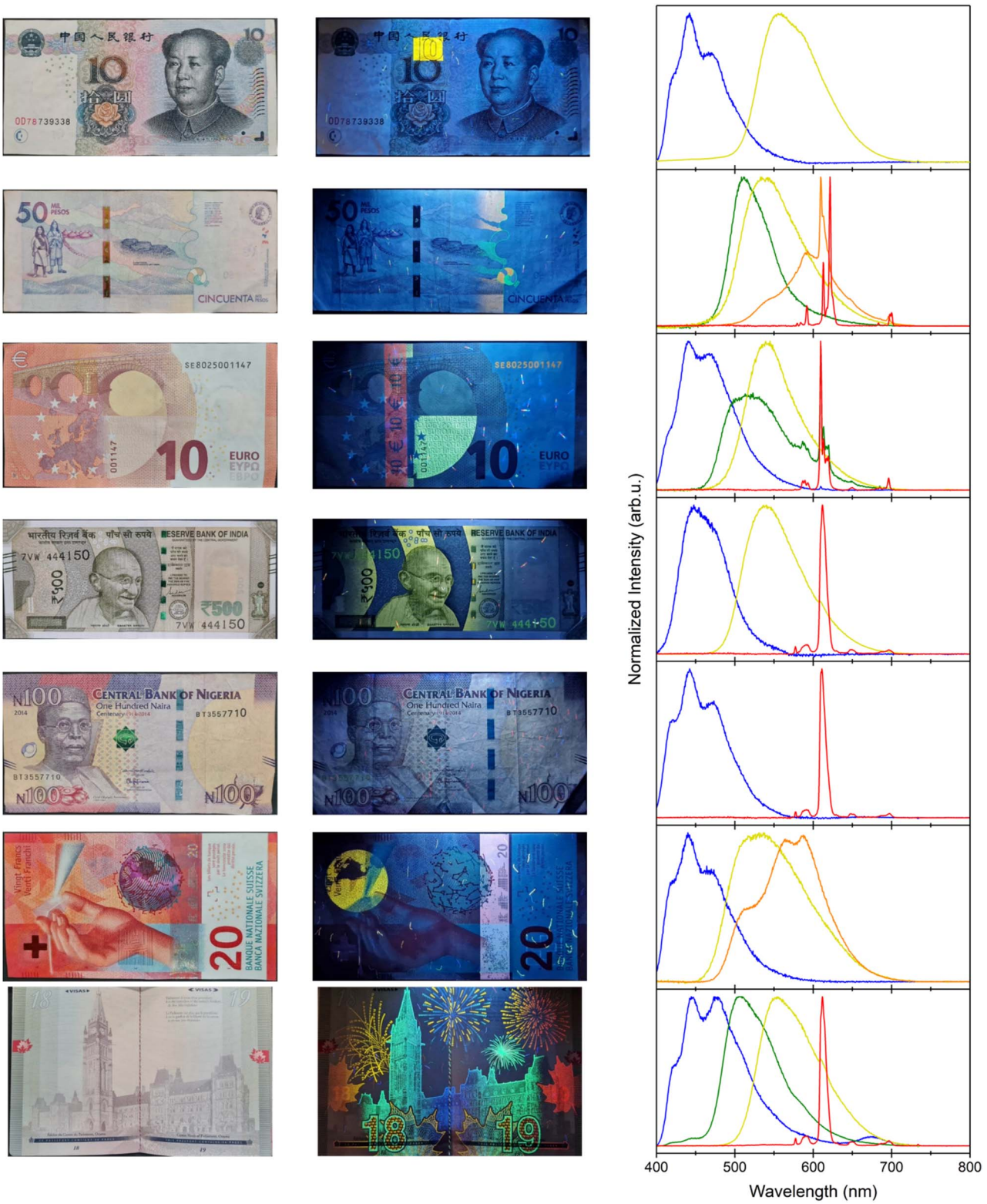

Fig. 5 Banknotes and documents from several countries (Left) photographed under ambient lighting, (Center) photographed under UV lamp irradiation (λ_{max}: 365 nm) and (Right) recorded emission spectra of the various observed phosphors. Chosen documents (from top to bottom) are 10 Chinese yuan, 50 000 Colombian pesos, 10 euro, 500 Indian rupees, 100 Nigerian naira, 20 Swiss francs, and a visa page from the Canadian passport.

security purposes, the exact composition of the different phosphors is not publicized. However, it is evident that the narrow bands from the red-emitting features on all the analyzed banknotes and documents in Fig. 5 are characteristic of Eu^{3+}. Because these transitions originate from the shielded electrons in the 4f orbitals of Eu^{3+}, their band positions do not vary greatly with host. Whether this ion is coordinated to organic molecules or doped in an inorganic material, these bands are unique to the $^5D_0 \rightarrow {}^7F_J$ transitions ranging between 575 and 750 nm.[205,206] Rather, the observed splitting patterns can change depending on the Eu^{3+} environment. Previous reports on the identity of the red Eu^{3+} luminescence in the euro suggest that an 8-coordinated complex is used, containing three bidentate β-diketone moieties.[207,208] A commonly studied ligand that results in a similar emission splitting pattern is 2-thenoyltrifluoroacetone (TTA), which can be paired with a variety of other ligands to fulfill the 8-fold coordination.[209,210]

The use of ligands to form complexes has some advantages. In comparison to other lanthanide 4f → 4f transitions, the Eu^{3+} emissions from the $^5D_0$ excited state are some of the most efficient, with quantum yields typically around 50%.[211,212] This is important as the more efficient a phosphor or luminescent species, the less of it is required in a spectroscopic taggant, which minimizes the cost. Nevertheless, Eu^{3+} and the other lanthanides have weak absorption cross-sections, which are magnitudes lower than fluorescent organic molecules. The use of spectroscopically active ligands, such as TTA, overcomes this issue by absorbing the incident ultraviolet light and transferring the energy to the Eu^{3+} metal center non-radiatively *via* the antenna effect.[213–216] This results in efficient luminescent complexes exploited for their bright red emissions.

Interestingly, these Eu^{3+} complexes are quite versatile. While the splitting patterns of the Eu^{3+} $^5D_0$ emissions between the euro and the other red-emitting documents are very different, the peak positions match perfectly with the Indian rupee, the Nigerian naira, and the Canadian passport. When Eu^{3+}(TTA) complexes are electrospun into polymer fibers, such as poly(-vinyl pyrrolidone), the environment surrounding the Eu^{3+} ions changes.[217–219] This results in the observed differences in the red emission spectra of Fig. 5, where the discrete band splitting broadens. The $^5D_0 \rightarrow {}^7F_0$ emission at 578 nm also appears, which is indicative of a low symmetry environment not present in the native complex.[205] The incorporation of these complexes within a polymer matrix improves its thermal and photostability, which is of utmost importance to the longevity of the security feature in something as manhandled as banknotes.

In contrast to the Eu^{3+} complexes, the Colombian peso elects to use a different red emitter entirely. The splitting pattern is reminiscent of an oxysulfide composition, such as Y_2O_2S or Gd_2O_2S.[220,221] When doped with Eu^{3+}, these materials are commonly used in lighting applications, such as cathode ray tubes and imaging detectors as discussed above.[222–224] Eu^{2+}-doped oxysulfide compositions are extremely photostable, which is why their widespread use in a variety of different industrial phosphor applications is so common.

All the documents recorded herein incorporate a similar blue luminescent phosphor, with distinct but overlapping emission bands. Previous reports have alluded to a $(BaO)_x \cdot 6Al_2O_3$ material doped with 2 to 15 mol% Eu^{2+}.[207,208] When $x = 0.82$, the phosphor has an emission maximum at 440 nm, and other values of x slightly shift the emission band.[225] Therefore it was speculated that the industrial synthesis of this phosphor results in phase-impure particles, resulting in a primary band at 440 nm that overlaps with a more broad band spanning from 410 to 525 nm. Through the use of Eu^{2+}, the allowed 5d → 4f transitions vary with the host, and facilitate a favorable emission in the blue region when doped into aluminate or silicate materials.[226] These oxide-based materials are common in lighting applications (Section 2), owing to their quantum yields that can exceed 70%.[227,228]

The recorded green and yellow phosphors are more difficult to determine since the emission spectra do not have any defining features. The choice of inorganic phosphor that may be responsible for such emissions can only be speculated as a potential option. A likely candidate that has previously been suspected of being in the euro is $SrGa_2S_4$:Eu^{2+}.[207] This material has multiple sites for the Eu^{2+} ion, creating a broadband emission centered in the green region of light with emission intensities similar to common phosphor materials in lighting applications.[229–232] A commonly used yellow phosphor in lighting applications is Ce^{3+}-doped $Y_3Al_5O_{12}$ (YAG), with an emission spectrum ranging from 500 to 650 nm, and quantum yields that exceed 80%.[233–235] Therefore, it is not too farfetched to consider these materials as likely candidates for the green and yellow features, respectively, present in the recorded documents.

Contrarily, the orange phosphors have many overlapping features and emission maxima, making them equally difficult to determine. For example, the iconic *Cittarium pica* on the Colombian peso consists of some characteristic Eu^{3+} signals, but in a different composition from what was discussed previously, overlapping a broader emission band spanning 500–700 nm.[236] Similarly, the globe feature on the Swiss franc contains multiple emission maxima between 475 and 700 nm. These bands can possibly, but not unequivocally, be attributed to materials co-doped with Mn^{2+} and Eu^{2+}, which possess similar emission spectra when doped into phosphates.[237–239]

It is interesting to observe the wide variety of colors that exist in different documents as a means of anti-counterfeiting, with many different lanthanide complexes and phosphors available. When weaved into the paper fibers, these banknotes and documents become exceedingly difficult to replicate. Only with specialized equipment and expertise is it even possible to observe, let alone reproduce, such complicated security measures. When corroborated with other features, such as the aforementioned serial number and PUFs, or even non-luminescent features, it becomes clear how determined governments and private industry manufacturers are to prevent forging, and how willingly they invest heavily with the purpose of limiting counterfeiting.

6 Telecommunications

As technology has developed over the last century, the internet and other means of communicating information across the

globe has advanced at a commensurate rate. Historically, copper wires pulsing an electric current conveyed information in the form of binary sequences. However, the development of optical fibers in the 1970s by Corning researchers Donald Keck, Robert Maurer, and Peter Schultz revolutionized the method through which data is communicated.[240,241] By exploiting pulses of light instead of electric currents, today's telecommunications technology can be transferred over larger distances with greater speed, less signal loss, larger bandwidths, and are designed more practically for industrial use (Fig. 6).[242–244]

Optical fibers exploit the use of high-purity fused silica for light propagation.[245] The core is composed of fused silica doped with an impurity such as germanium dioxide or chlorine, to increase the refractive index which achieves total internal reflection.[246] Semiconductor diode lasers act as the light source in optical signals because of their compact size and range of potential wavelengths.[247] The choice of wavelengths used in optical telecommunication is dependent on the absorption coefficient of the fused silica, which is lowest in the near-infrared (NIR) region. Ranging from 1260 to 1625 nm, the attenuation of light through the optical fiber materials is less than 0.5 dB km^{-1}, which is very important for long-distance data transfer.[247] Within this range, two bands are the most widely used, the O-band between 1260 and 1360 nm, and the C-band between 1530 and 1565 nm.[248] While the O-band has higher attenuation in fused silica, the C-band is subject to greater chromatic dispersion, which distorts and can possibly overlap pulses of the incoming signal. Therefore, the O-band is specifically used in shorter-distance information transfer, while the C-band is exploited in long and ultra-long haul telecommunication applications.

Despite these advancements in the transmission of information, light signals confined to the inside of optical fibers are still subject to losses over distances that exceed 100 km.[249] Amplifiers overcome this dilemma by periodically increasing the signal intensity, improving data transfer from the transmitter to the receiver. Traditional amplification involved the conversion of light signals to electric current that could then be amplified before converting back to light.[250] This process was impractical and slow, acting as a bottleneck that greatly limited transfer speeds. The use of lanthanides in optical amplifiers was introduced in the late 1980s as a faster alternative.[249] Given the abundance of potential energy levels in trivalent lanthanides, the study and use of fiber amplifiers have included ions of neodymium, praseodymium, holmium, erbium, thulium, and ytterbium, which all have excitation and emission bands in the NIR region of light.[251–256] Following the basic premise of a laser, lanthanide ions doped into an optical fiber could be excited using an external laser source (separate from the telecommunication signal).[257] The long-lived excited states help facilitate population inversion, and the incoming photons from the information signal induce a stimulated emission. This stimulated emission results in more photons that are in-phase and monochromatic with the telecommunication signal, and since the signal does not need to be converted to an electric current, faster amplification is achieved.

First discovered in 1987, the erbium-doped fiber amplifier (EDFA), which consists of fused silica fibers doped with Er_2O_3, is still the most commonly used optical signal amplifier today.[258] EDFAs increase the signal intensity of data transmissions operating in the C-band, due to the efficient $^4I_{13/2} \rightarrow {}^4I_{15/2}$ emission of Er^{3+} at 1550 nm.[259–261] When excited using a 980 nm laser, the Er^{3+} ions are promoted into the $^4I_{11/2}$ excited state. This ion then relaxes non-radiatively to populate the $^4I_{13/2}$ level. When the excitation source is of sufficiently high energy, there is an accumulation of Er^{3+} ions excited into this state, achieving the necessary population inversion to properly amplify the subsequent data signals. Once a data signal (with a wavelength of approximately 1550 nm) interacts with the excited Er^{3+}, the ion relaxes to the ground state, ejecting an electron in-phase with the original optical signal. High-power amplifiers use 1480 nm as the Er^{3+} excitation source instead (populating a sublevel of the $^4I_{13/2}$ state).[259,262] This excitation wavelength has a lower absorption cross-section than 980 nm, but under certain conditions can outperform the amplification capabilities from 980 nm excitation.

When data transfer is not required to travel extended distances (<100 km), the O-band is preferred, with wavelengths around 1300 nm, which are not as susceptible to chromatic dispersion compared to the C-band.[248] Praseodymium-doped fiber amplifiers (PDFAs) based on silica or fluoride compounds are used as signal amplifiers instead, owing to the resonance in this wavelength region.[263–265] Similar to EDFAs, the Pr^{3+} ions are excited into the $^1G_4$ state using an external $\approx$1000 nm laser source. Incoming signal photons of 1300 nm can then induce stimulated emission of the $^1G_4 \rightarrow {}^3H_5$ transition, amplifying the signal. Interestingly, the energy levels of Pr^{3+} help facilitate population inversion, more so than Er^{3+}, since the 1300 nm emission does not relax the ions to the $^3H_4$ ground state, which follows the premise of a four-level laser.[266] However, the quantum efficiency of the $^1G_4 \rightarrow {}^3H_5$ transition is low, as compared to Er^{3+}, due to multiphonon relaxation processes that quench the $^1G_4$ excited state to lower-lying states.

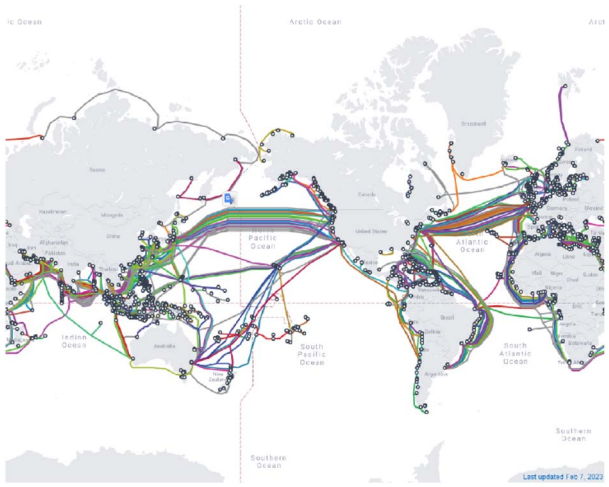

Fig. 6 Map of the submarine telecommunications cables around the world as of 2023. Reproduced from https://www.submarinecablemap.com/.

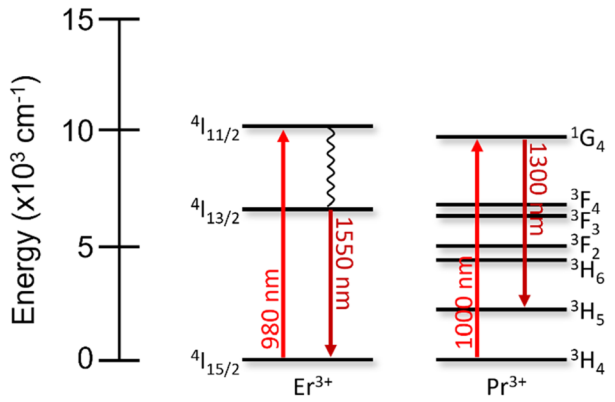

Fig. 7 Energy level diagrams of Er^{3+} and Pr^{3+} depicting the excitation and emission wavelengths relevant for their use in optical amplifiers.

These intermediate states are not present below the emitting $^4I_{13/2}$ level of Er^{3+} (Fig. 7). These subtle differences in EDFAs and PDFAs influence the way they are engineered to overcome their respective shortcomings.

As the demand for faster telecommunication speeds increases, recent studies aim to further advance the way optical information signals are transmitted. One such advancement is the use of polymeric optical fibers instead of the traditional fused silica.[267,268] Polymeric fibers are less expensive to manufacture, lighter, and more flexible than silica.[269] However, since phonon quenching is a common drawback to lanthanide luminescence, the abundance of O–H, N–H, and C–H vibrations that are present in polymer materials hinder their effectiveness as optical amplifiers. Moreover, the approach to incorporating lanthanides in polymers must also be modified, since inorganic oxides will not be suitable. Lanthanide complexes with fluorinated ligands have emerged as the preferred option, owing to weaker vibrational modes from C–F bonds rather than C–H bonds.[270,271] However this technology is still in its infancy, since the signal amplification is still not sufficient to compare with traditional EDFAs.

Newly emerging erbium-doped waveguide amplifiers (EDWAs) are showing promise in advancing signal amplification in optoelectronics.[272] These devices consist of lanthanide complexes embedded within silica and polymers on a silicon substrate.[267,273] Following the same optical amplification technology as EDFAs, EDWAs are directly manufactured into integrated circuit boards, avoiding the need for external signal amplification. As our reliance on global communication increases, it will likely become necessary to develop materials which are capable of transmitting data of even larger sizes at even faster rates. Likely, lanthanides will continue to aid in facilitating the next generation of telecommunication technologies.

7 Next-generation technologies

7.1 Solar energy conversion

Currently, the spectral mismatch between the materials used in solar cells and the solar emission spectrum represents a major obstacle to increasing the efficiency of existing photovoltaic (PV) cells (Fig. 8).[274] For example, the maximum absorption by silicon PV cells is only 48% of the total solar emission, since they absorb in the range of approximately 400–1200 nm, whereas the entire solar emission spectrum ranges approximately 250–2500 nm. Moreover, the most efficient conversion of solar energy to electricity occurs when the semiconductor absorbs light at wavelengths closest to its intrinsic bandgap. Thus, silicon, GaAs and halide perovskite PVs are most efficient around 900–1100 nm but can also less-efficiently absorb visible light.[275–277] Lanthanide-based spectral wavelength converting technology has the potential to expand our ability to harness additional wavelengths from the solar spectrum.[274–276] In this way, lanthanides are mostly used in complementary technologies or in direct combination with silicon PV devices, since those are already well-established in the commercial market. Less commonly, lanthanides incorporated into the semiconductor components of PV cells are also under investigation and have been patented.[278,279] Organic polymers and dyes represent the main alternative to lanthanides in the solar industry and are substantially less expensive. However, the photostability of lanthanide-based materials represents an important advantage that may justify the added cost of their use.[275,276,280,281] At this time, widespread commercial use of lanthanide luminescence in solar energy conversion has not been realized. However, there are many active patents toward the development of such technologies, and we aim to focus this discussion on conclusions we can base on the research that has made it to the patent stage. The interested reader is directed to several publications that provide an in-depth discussion on the state of the field based on academic literature.[274–276,278,282]

Lanthanides can absorb solar wavelengths otherwise not absorbed by the PV cells, and re-emit them at longer or shorter wavelengths, through quantum cutting (QC)/downshifting (DS) or upconversion (UC) processes, respectively (Fig. 8).[274,283] These newly emitted photons can then be absorbed by the PV cells, improving their solar harnessing capabilities. The process of upconversion involves the absorption of two or more low energy photons which are converted into a higher-energy photon. In this way, NIR light that is lower than the bandgap energy of the PV semiconductor (>1100 nm in the case of silicon) can be harnessed and converted to wavelengths suitable for bandgap excitation. On the contrary, in QC/DS, a higher-energy photon is converted into one or more low energy photons.[6] In this way, the UV and visible wavelengths are harnessed and converted to longer wavelengths. The characteristic narrow emission bands from the 4f → 4f transitions of Ln^{3+} ions fulfill the requirements for the conversion of the broad solar spectrum to a narrow emission range at wavelengths suitable for commercial PVs.

First patented by Renata Reisfeld in 1979, lanthanide-based luminescent solar concentrators (LSC) work by absorbing solar energy over a large surface area, transforming it into a fluorescent emission, and then focusing the light onto a smaller target which is then harnessed by PVs at the edge of the LSC.[276,284] LSCs are usually transparent and can be multilayered to achieve the use of a wider range of the solar spectrum by incorporating

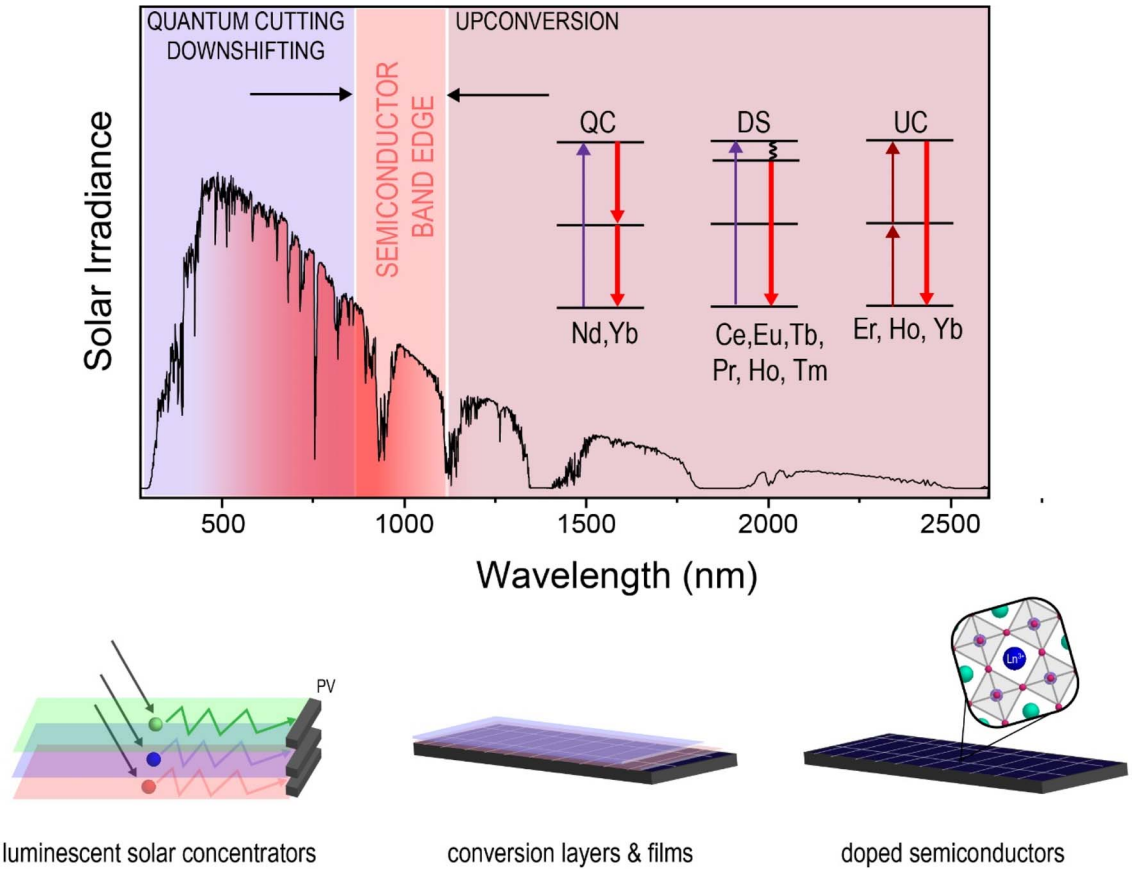

Fig. 8 Solar energy conversion technologies using lanthanides. The solar irradiance spectrum (top) and corresponding regions of wavelengths where upconversion, quantum cutting and downshifting can be harnessed. Inset shows the mechanisms relevant to each of the luminescence mechanisms. On the bottom, there are graphical depictions of luminescent solar concentrators (left), photovoltaic conversion layers and films (middle) and photovoltaic cells doped with lanthanides directly into the semiconductor layer.

different lanthanides into different layers.[277,284,285] This type of technology is particularly interesting for urban applications where LSCs can be incorporated into building architecture, especially in windows since LSCs require large surface areas to operate.[276] In a similar fashion, many patented technologies use transparent lanthanide films as layers directly on PV surfaces.[286–289] In both technologies, specific lanthanides are more successful either for UC or QC/DS; the main difference is simply whether the lanthanide components are used in tandem with a PV cell or directly coated onto one.

NIR light is harvested and transformed to useable wavelengths *via* UC, with most technologies using Er^{3+} or Er^{3+} and Yb^{3+} together. In this way, Er^{3+} can absorb wavelengths around 1550 nm, and emit at 980 nm upon sequential absorption, which is close to the band edge of silicon. Similarly, both Er^{3+} and Yb^{3+} can absorb 980 nm photons, resulting in the emission of green light from Er^{3+} that is well-absorbed by GaAs PVs. Several layered PV designs are under active patents using Er^{3+} and Er^{3+}/Yb^{3+}.[288,290,291] These ions are also well-established in the literature and appear to be the optimal choices for harnessing NIR light in PV devices.[274–276] To our knowledge, there are few active patents involving lanthanide-based layers as upconversion layers in LSCs, and they also use Er^{3+} and/or Yb^{3+}.[277,285]

Upconversion is substantially more limited in efficiency than QC/DS, as expected from an anti-Stokes process. For this reason, there are substantially more examples of lanthanides as QC/DS converters. Eu^{3+} is perhaps the most well-established for solar QC/DS, taking advantage of UV light, since its red emissions are closer to the desired wavelengths, and some Eu^{3+} complexes have particularly impressive quantum efficiencies relative to other lanthanides.[275,287,292] In many cases, the antenna effect is particularly useful, in which the ligand (having a higher absorption cross-section than the lanthanides) absorbs the incident solar light and transfers it to the lanthanide metal center.[277,287,292] Tb^{3+} complexes are the second-most promising for QC/DS, as they also efficiently absorb UV light, but convert it to green light, which is somewhat less desirable for use with a silicon solar cell but is still efficient for the excitation of GaAs PVs.[284] Notably, the luminescence of Tb^{3+} and Eu^{3+} complexes was reported to be significantly enhanced by noble metal nanoparticles due to plasmon resonance.[274,276,277] Nd^{3+}-Yb^{3+} complexes are also able to harvest blue light and convert it to NIR *via* QC at 980 nm, even closer to the intrinsic bandgap of silicon than the Eu^{3+} emissions.[293] The QC process occurs *via* energy transfer from Nd^{3+} to Yb^{3+}, following the mechanism [Nd^{3+} ($^4G_{9/2} \rightarrow {}^4F_{3/2}$); Yb^{3+} ($^2F_{5/2} \leftarrow {}^2F_{7/2}$)], followed by a second

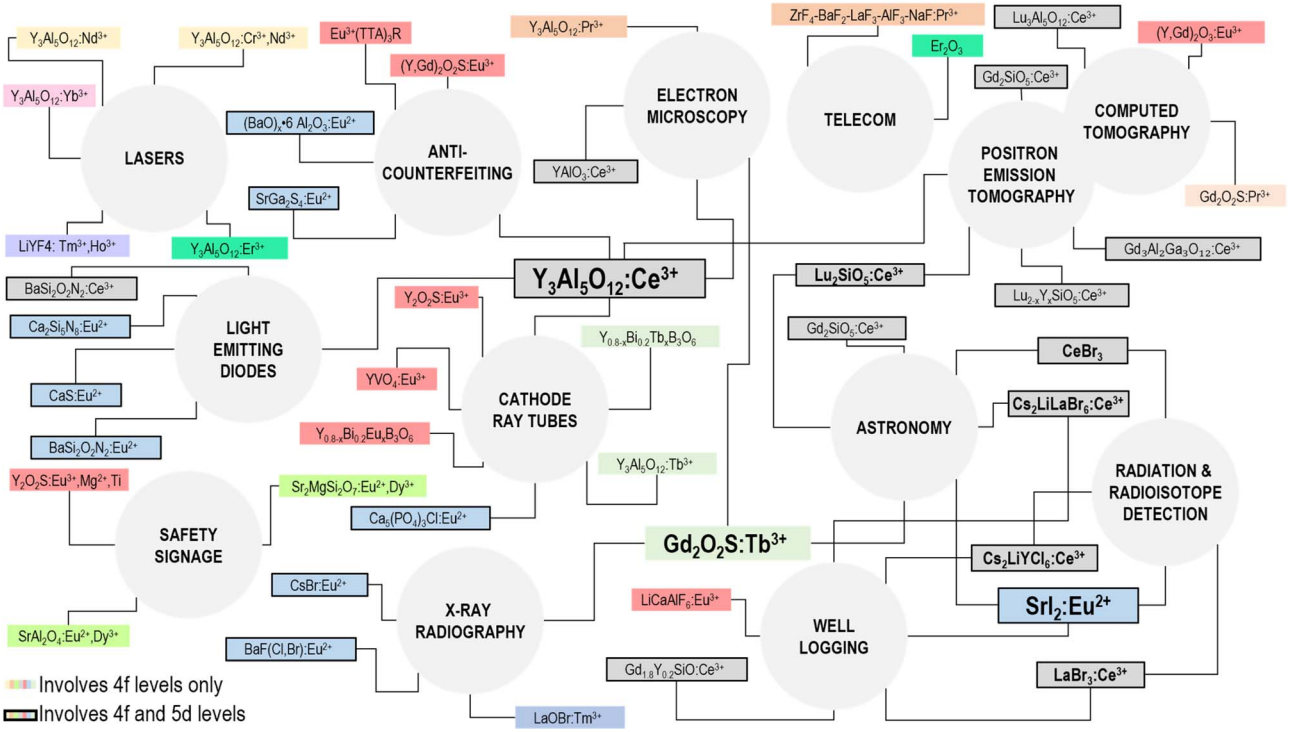

Fig. 9 Summary scheme depicting the phosphors and materials mentioned throughout this review.

energy transfer from the $Nd^{3+}(^4F_{3/2})$ level to the $Yb^{3+}(^2F_{5/2})$ level, yielding two NIR photons from Yb^{3+}. In theory, QC is particularly attractive because of the potential to achieve quantum efficiencies greater than 100%.[275] In practice, the efficiencies are closer to a one-to-one process like DS. Ce^{3+} complexes are also proposed for their incorporation in LSCs in combination with other lanthanides such as Eu^{3+} and Tb^{3+}, whereby Ce^{3+} can absorb UV light and energy transfer to the Eu^{3+} and Tb^{3+} complexes which then emit at more appropriate wavelengths.[277] In some instances, the radiative 5d → 4f transitions of Ce^{3+} can be found in the green region, and thus Ce^{3+} can be directly used as a wavelength-converting ion. This has been proposed with YAG:Ce^{3+}, as well as with Ce^{3+}-doped perovskite quantum dots.[294,295] PV devices based on halide perovskites have become quite attractive and are likely to be explored further for commercial translation. Notably, lanthanide-doped perovskite solar cells have gained momentum since 2015, reaching solar cell efficiencies around 20%.[275,278] Most of the perovskite PV devices also employ Eu^{3+}, Er^{3+}, and Yb^{3+}, though nearly all lanthanides have been assessed for incorporation into perovskite lattices or in films on top of a perovskite active layer.

Lanthanide-based solar technologies have been under development for nearly half a century, but have not yet reached widespread commercial adaptation.[292] Advancements in improving the efficiencies of these materials are continually sparking new developments in the technologies making use of lanthanides, and suggest that there is still great potential for them in the commercial market. The photostability of lanthanide materials and the narrow emission bands from the 4f → 4f transitions of these ions are strong advantages over alternative technologies employing strictly organic molecules. Likely, hybrid organic-inorganic technologies will pave the way for commercial adaptations of lanthanide luminescence in the solar industry.[286] If cost-efficiency barriers are adequately addressed, lanthanides will likely progress our abilities to efficiently harness the UV and infrared regions of the solar spectrum. However, this is a prime example of how cost-benefit evaluations are crucial for the introduction of an invention, no matter how promising it is.

7.2 Alternative lighting technologies

The application of lanthanide-based phosphors can provide benefits in several other industrial sectors. For military and space applications, the challenge to obtain produce in space is contingent on finding the right lighting system.[296] Several kinds of crops and vegetables have been exposed to light with a different spectral distribution to verify the best growth conditions.[297–299] Well-established products, such as white-light lightbulbs (as discussed in Section 2) that mimic the spectral characteristics of the sun for plant growth indoors, are also promising for farming in space. Obtaining a self-sustained ecosystem to support life in space is a recurring idea in recent years, which can potentially bring more lanthanides to outer space.

Finally, the possibility to achieve lighting without additional energy consumption with persistent luminescence is quite attractive, but still far from being realized. Finally, the phenomenon of persistent luminescence should also be considered in view of its usefulness for safety signals and

panels.[27] In a material with an intermediate trapping state positioned appropriately within a band gap, the trap state can accumulate trapped charges during irradiation of the considered persistent luminescent phosphor. When irradiation ceases, the charges are released, producing persistent luminescence (also known as afterglow). The most efficient of these phosphors are $Sr_2MgSi_2O_7$:Eu^{2+},Dy^{3+} (blue), $SrAl_2O_4$:Eu^{2+},Dy^{3+} (green) and Y_2O_2S:Eu^{3+},Mg^{2+},Ti (red).[27] Persistent phosphors have found commercial use in everything from watch dials and glow-in-the-dark toys to emergency safety signage on buildings, passenger trains, and naval ships among others.[300–303] Notably, $SrAl_2O_4$:Eu^{2+},Dy^{3+} signs have been used to replace radioactive tritium signs at military stations, thereby improving the safety of personnel.[303] With respect to persistent luminescence duration, major optimizations have already been realized, achieving emissions that exceed 12 h. This certainly suffices in terms of replacing lighting in the absence of the sun (*i.e.* at night). However, the intensity of the emissions, and their color, require substantial improvements. Sunlight-activated persistent luminescent phosphors are nevertheless appearing in the literature, making them a foreseeable perspective for the future of lighting.[304] Given that most of the modern persistent luminescent material advancements were made starting in the 1990s,[305,306] the field is relatively young and thus there is still much to be learned towards making this a feasible lighting technology.

8 Conclusions

Lanthanide luminescence is ubiquitous in modern society, from under the oceans to deep space, since they have facilitated an incredible variety of technologies. Despite the difficulties faced in isolating and identifying these elements, as well as the uncertainties faced in their supplies, the modern world has become reliant on the lanthanides.

The unparalleled narrow band emissions of the trivalent lanthanides have facilitated lighting and displays with high color purity and have allowed for the precise conversion of broad solar wavelengths to specific and useful emissions that can be harnessed by semiconductors in photovoltaic cells. Simultaneously, the broad 5d → 4f transitions have vastly improved the phosphor and scintillator industries.

With regard to the medical industry, the luminescent properties of the lanthanides have been crucial in everything from laser ablation in ophthalmologic surgery, to tattoo removal, to medical imaging in X-ray, PET and CT scanning. Moreover, their use in solid-state lasers has enabled wireless communications, facilitating the possibility for deep space communication and allowed us to monitor the atmosphere of the earth *via* LIDAR technologies from space. Lanthanides are also integrated in our everyday lives in the form of luminescence-based anti-counterfeiting in money and passports. The phosphors employed throughout these applications, incorporating the lanthanides as a dopant or part of the native composition, are summarized in Fig. 9, depicting their range as well as their versatility.

As advancements are made in mining technologies, and more countries introduce rare-earth mining operations, the potential for stable supplies of lanthanides, as well as a decrease in their cost may occur. Notably, the lanthanides are not only prized for their luminescence properties, thus there are many additional reasons they are coveted. Solving these issues will likely spur the industry into taking advantage of the unique properties of these elements. Throughout this review, we aimed to provide an overview of how lanthanide luminescence has benefitted society, so that their historical uses and their use in today's technologies may inspire future researchers to harness lanthanide luminescence in the next generation of the modern era.

Author contributions

G. T. and G. A. M. contributed equally. All authors curated the references and wrote and edited the manuscript.

Conflicts of interest

There are no conflicts of interest to declare.

Acknowledgements

J. A. C. is a Concordia University Research Chair in Nanoscience and is grateful to Concordia University for financial support. J. A. C. is grateful to the Natural Science and Engineering Research Council (NSERC) of Canada for the sustained support of his research (No. RGPIN-2022-04704). G. T. is grateful to the Université Laval for financial support. S. L. M. and G. A. M. are grateful to NSERC for financial support through the Alexander Graham Bell graduate scholarships. S. L. M. is grateful for financial support from Concordia University's doctoral incentive fellowship. M. K. is grateful to Concordia University for financial support through the Tuition Award of Excellence.

References

1 E. F. Worden, R. W. Solarz, J. A. Paisner and J. G. Conway, *J. Opt. Soc. Am.*, 1978, **68**, 52–61.
2 F. J. Gustafson and J. C. Wright, *Anal. Chem.*, 1979, **51**, 1762–1774.
3 J. C. Wright, *Anal. Chem.*, 1977, **49**, 1690–1702.
4 L. Tansjö, in *Episodes from the History of the Rare Earth Elements*, ed. C. H. Evans, Springer Netherlands, Dordrecht, 1996, vol. 15, pp. 37–54.
5 *Section 14: Geophysics, Astronomy and Acoustics*, ed. J. R. Rumble, CRC Press/Taylor & Francis, 2022.
6 R. Eggert, C. Wadia, C. Anderson, D. Bauer, F. Fields, L. Meinert and P. Taylor, *Annu. Rev. Environ. Resour.*, 2016, **41**, 199–222.
7 J. G. Bünzli, *Eur. J. Inorg. Chem.*, 2017, 5058–5063.
8 D. N. Woodruff, R. E. P. Winpenny and R. A. Layfield, *Chem. Rev.*, 2013, **113**, 5110–5148.
9 J. A. Cotruvo, *ACS Cent. Sci.*, 2019, **5**, 1496–1506.

10 J. C. G. Bünzli and C. Piguet, *Chem. Soc. Rev.*, 2005, **34**, 1048–1077.
11 M. Shibasaki and N. Yoshikawa, *Chem. Rev.*, 2002, **102**, 2187–2209.
12 R. T. Wegh, H. Donker, K. D. Oskam and A. Meijerink, *Science*, 1999, **283**, 663–666.
13 T. Senden, F. T. Rabouw and A. Meijerink, *ACS Nano*, 2015, **9**, 1801–1808.
14 C. Ronda, *J. Lumin.*, 2002, **100**, 301–305.
15 C. Ronda, *Prog. Electromagn. Res.*, 2014, **147**, 81–93.
16 United States Patent Office, *US Pat.*US234345A, 1880.
17 C. J. Cleveland and C. G. Morris, *Handbook of Energy. Volume II_ Chronologies, Top Ten Lists, and Word Clouds*, Elsevier, 2014.
18 F. Hauksbee, *Philos. Trans. R. Soc. London*, 1705, **24**, 2129–2135.
19 R.-S. Liu and X.-J. Wang, *Phosphor Handbook*, CRC Press, Boca Raton, 2021.
20 United States Patent Office, *US Pat.*US2182732A, 1927.
21 L. Ozawa and M. Itoh, *Chem. Rev.*, 2003, **103**, 3835–3855.
22 A. K. Levine and F. C. Palilla, *Appl. Phys. Lett.*, 1964, **5**, 118–120.
23 J. R. McCOLL and F. C. Palilla, in *Industrial Applications of Rare Earth Elements*, American Chemical Society, 1981, pp. 177–193.
24 United States Patent Office, *US Pat.*US2748303A, 1949.
25 United States Patent Office, *US Pat.*US3440080A, 1969.
26 United States Patent Office, *US Pat.*US3418246A, 1968.
27 United States Patent Office, *US Pat.*US3394084A, 1968.
28 United States Patent Office, *US Pat.*US3989977A, 1976.
29 Y. Gao, P. Jiang, W. Gao, R. Cong and T. Yang, *J. Solid State Chem.*, 2019, **278**, 120915.
30 N. Katoh, T. Deguchi and R. S. Berns, *Opt. Rev.*, 2001, **8**, 305–314.
31 J. Ballato, J. S. Lewis III and P. Holloway, *MRS Bull.*, 1999, 51–56.
32 Thomas Electronics, 2023, **https://www.thomaselectronics.com/avionics/head-up-display/**, accessed June 5 2023.
33 C. Ronda and A. Srivastava, *Electrochem. Soc. Interface*, 2006, **15**, 55–57.
34 R. Marin and D. Jaque, *Chem. Rev.*, 2021, **121**, 1425–1462.
35 A. Tiwari and S. J. Dhoble, *Luminescence*, 2020, **35**, 4–33.
36 S. Jin, R. Li, H. Huang, N. Jiang, J. Lin, S. Wang, Y. Zheng, X. Chen and D. Chen, *Light Sci. Appl.*, 2022, **111**, 1–13.
37 United States Patent Office, *US Pat.*US3819974A, 1973.
38 Z. Xia and Q. Liu, *Prog. Mater. Sci.*, 2016, **84**, 59–117.
39 United States Patent Office, *US Pat.*US8597543B2, 2012, 347.
40 United States Patent Office, *US Pat.*US9530944B2, 2015.
41 United States Patent Office, *US Pat.*US7352006B2, 2004.
42 European Patent Office, EP1837386B1, 2005.
43 United States Patent Office, *US Pat.*US7250715B2, 2004.
44 United States Patent Office, *US Pat.*US7951308B2, Partial English Transl. Off. Action issued Sep, 2010, vol. 29, p. 624.
45 A. Dunselman, *Lighting world first: Philips breaks 200 lumens per watt barrier*, 2013.
46 M. Richi, *Success in research: First gallium-nitride LED chips on silicon in pilot stage*, Munich. Germany, 2012.
47 M. Kawa and J. M. J. Fréchet, *Chem. Mater.*, 1998, **10**, 286–296.
48 M. Kaur, G. A. Mandl, S. L. Maurizio, G. Tessitore and J. A. Capobianco, *Nanoscale Adv.*, 2022, **4**, 608–618.
49 M. Pietraszkiewicz, M. MacIejczyk, I. D. W. Samuel and S. Zhang, *J. Mater. Chem. C*, 2013, **1**, 8028–8032.
50 G. L. Law, K. L. Wong, H. L. Tam, K. W. Cheah and W. T. Wong, *Inorg. Chem.*, 2009, **48**, 10492–10494.
51 J. H. S. K. Monteiro and A. De Bettencourt-Dias, *Lanthanide-Based Multifunct. Mater. From OLEDs to SIMs*, 2018, pp. 99–131.
52 J. M. Ha, S. H. Hur, A. Pathak, J. E. Jeong and H. Y. Woo, *NPG Asia Mater.*, 2021, **13**, 1–36.
53 L. Wang, Z. Zhao, C. Wei, H. Wei, Z. Liu, Z. Bian and C. Huang, *Adv. Opt. Mater.*, 2019, **7**, 1801256.
54 A. De Bettencourt-Dias, *Dalton Trans.*, 2007, 2229–2241.
55 United States Patent Office, *US Pat.*US04168012, 1962.
56 F. Jobin, P. Paradis, Y. O. Aydin, T. Boilard, V. Fortin, J.-C. Gauthier, M. Lemieux-Tanguay, S. Magnan-Saucier, L.-C. Michaud, S. Mondor, L.-P. Pleau, L. Talbot, M. Bernier and R. Vallée, *Opt. Express*, 2022, **30**, 8615.
57 A. A. Kaminskii, *Phys. Status Solidi*, 1985, **87**, 11–57.
58 B. M. Walsh, N. P. Barnes, M. Petros, J. Yu and U. N. Singh, *J. Appl. Phys.*, 2004, **95**, 3255–3271.
59 D. W. Ball, *Field Guide to Spectroscopy*, SPIE Press, Bellingham, 2006.
60 United States Patent Office, *US Pat.*US3252103A, 1964.
61 U. Keller, *Nature*, 2003, **424**, 831–838.
62 United States Patent Office, *US Pat.*US13/562,045, 2012.
63 China National Intellectual Property Administration, CN94115013A, 1994.
64 United States Patent Office, *US Pat.*US6621040B1, 1997, 522.
65 World Intellectual Property Organization, WO2007092803A2, 2007.
66 United States Patent Office, *US Pat.*US10787517, 2004.
67 European Patent Office, EP15754589.8A, 2015.
68 European Patent Office, EP13709796.0A, Semicond. Disk Lasers, 2013.
69 United States Patent Office, *US Pat.*US10/231580, 2002.
70 M. Malinauskas, A. Žukauskas, S. Hasegawa, Y. Hayasaki, V. Mizeikis, R. Buividas and S. Juodkazis, *Light Sci. Appl.*, 2016, **58**(5), e16133.
71 United States Patent Office, *US Pat.*US4538608A, 1984.
72 C. S. Fong Sze-Un, *Singap. Med. J.*, 2007, **48**, 709–719.
73 United States Patent Office, *US Pat.*US10058388B2, 2018, p. 2.
74 United States Patent Office, *US Pat.*US11452638B2, 2019.
75 H. K. Soong and J. B. Malta, *Am. J. Ophthalmol.*, 2009, **147**, 189–197.
76 European Patent Office, EP2010087B1, 2007.
77 European Patent Office, EP4094876A1, 2014.
78 United States Patent Office, *US Pat.*US9254174B2, 2013.
79 European Patent Office, EP2838613B1, 2013.
80 China National Intellectual Property Administration, CN105120787B, 2014.

81 U. Hohenleutner, S. Hohenleutner, W. Bäumler and M. Landthaler, *Lasers Surg. Med.*, 1997, **20**, 242–247.
82 J. T. Willie, J. K. Tung and R. E. Gross, ed. A. J. B. T.-I.-G. N. Golby, Academic Press, Boston, 2015, pp. 375–403.
83 United States Patent Office, *US Pat.*US20120215209A1, 2012.
84 L. Hernandez, N. Mohsin, F. S. Frech, I. Dreyfuss, A. Vander Does and K. Nouri, *Lasers Med. Sci.*, 2022, **37**, 2581–2587.
85 United States Patent Office, *US Pat.*US20150289935A1, 2015.
86 United States Patent Office, *US Pat.*US20060149223A1, 2005.
87 C. Raulin, W. Kimmig and S. Werner, *Hautarzt*, 2000, **51**, 463–473.
88 B. Greve and C. Raulin, *Dermatol. Surg.*, 2002, **28**, 156–161.
89 Y. S. Jang and S. W. Kim, *Nanomanuf. Metrol.*, 2018, **1**, 131–147.
90 L. D. Smullin and G. Fiocco, *Nature*, 1962, **194**, 1267.
91 L. Flannigan, L. Yoell and C. Q. Xu, *J. Opt.*, 2022, **24**(4), 043002.
92 D. M. Boroson, A. Biswas and B. L. Edwards, in *Free-Space Laser Communication Technologies XVI*, SPIE, 2004, vol. 5338, p. 16.
93 L. Ramos-Izquierdo, J. L. Bufton and P. Hayes, *Appl. Opt.*, 1994, **33**, 307.
94 D. E. Smith, M. T. Zuber, X. Sun, G. A. Neumann, J. F. Cavanaugh, J. F. McGarry and T. W. Zagwodzki, *Science*, 2006, **311**, 53.
95 B. Mathason, M. M. Albert, D. Engin, H. Cao, K. G. Petrillo, J. Hwang, K. Le, K. Puffenberger, S. Litvinovitch, R. Utano, M. Storm, M. Shelton, A. Pulkkinen and E. J. Summerlin, *33 st Annu. AIAA/USU Conf. Small Satell.*, 2019, SSC19-P3-2, 1–5.
96 A. Carrasco-Casado, F. Harrison, A. Biswas, R. Fields, B. Grefenstette, F. Harrison, S. Sburlan and M. Toyoshima, *IEEE Int. Conf. Sp. Opt. Syst. Appl.*, 2017, 46–52.
97 United States Patent Office, *US Pat.*US20070041083A1, 2005, p. 822.
98 F. Di Teodoro and C. D. Brooks, *Opt. Lett.*, 2005, **30**, 3299.
99 C. D. Brooks and F. Di Teodoro, *Opt. Lett.*, 2005, **30**(20), 2694–2696.
100 M. N. Zervas and C. A. Codemard, *IEEE J. Sel. Top. Quantum Electron.*, 2014, **20**, 219–241.
101 E. Cartlidge, *Physicists are planning to build lasers so powerful they could rip apart empty space*, **https://www.science.org/content/article/physicists-are-planning-build-lasers-so-powerful-they-could-rip-apart-empty-space**.
102 M. D. Perry and G. Mourou, *Science*, 1994, **264**, 917–924.
103 H. Hemmati, A. Biswas and I. B. Djordjevic, *Proc. IEEE*, 2011, **99**, 2020–2039.
104 B. J. Puttnam, R. S. Luís, G. Rademacher, Y. Awaji and H. Furukawa, *Opt. Fiber Commun. Conf.*, 2021, **2021**, F3B.3.
105 H. Zech, F. Heine and M. Motzigenmba, in *Proc. International Conference on Space Optical Systems and Applications (ICSOS)*, 2014, vol. 9, pp. 7–10.
106 Z. Sodnik, H. Lutz, B. Furch and R. Meyer, *Free. Laser Commun. Technol. XXII*, 2010, vol. 7587, p. 758705.
107 U. N. Singh and M. J. Kavaya, *Enabling Laser and Lidar Technologies for NASA's Science and Exploration Mission's Applications*, Hampton, 2002.
108 F. Fouladinejad, A. Matkan, M. Hajeb and F. Brakhasi, in *International Archives of the Photogrammetry, Remote Sensing and Spatial Information Sciences - ISPRS Archives*, 2019, vol. 42, pp. 407–414.
109 A. Fix, G. Naletto, I. Hutchinson, N. Karafolas, W. Riede, A. Heliere, B. Menzies and H. Riris, *CEAS Space J.*, 2019, **11**, 359–362.
110 G. J. Koch, B. W. Barnes, M. Petros, J. Y. Beyon, F. Amzajerdian, J. Yu, R. E. Davis, S. Ismail, S. Vay, M. J. Kavaya and U. N. Singh, *Appl. Opt.*, 2004, **43**, 5092–5099.
111 S. Chen, J. Yu, M. Petros, Y. Bai, U. N. Singh and M. J. Kavaya, in *Lidar Remote Sensing for Industry and Environmental Monitoring*, SPIE, 2005, vol. 5653, p. 175.
112 F. Amzajerdian, B. L. Meadows, N. R. Baker, R. S. Baggott, U. N. Singh and M. J. Kavaya, in *SPIE's Fourth International Asia-Pacific Environmental Remote Sensing Symposium*, Honolulu, HI, 2004.
113 M. J. Kavaya and G. David Emmitt, in *Laser Radar Technology and Applications III part od SPIE's Aerospace/Defense Sensing Controls*, Orlando, FL, USA, 1998.
114 C. Pierangelo, B. Millet, F. Esteve, M. Alpers, G. Ehret, P. Flamant, S. Berthier, F. Gibert, O. Chomette, D. Edouart, C. Deniel, P. Bousquet and F. Chevallier, in *EPJ Web of Conferences*, 2016, vol. 119.
115 G. Blasse, in *Springer Handbook of Electronic and Photonic Materials*, Springer International Publishing, Cham, 2017, p. 1.
116 A. Lempicki, A. J. Wojtowicz and C. Brecher, Inorganic Scintillators, in *Wide-Gap Luminescent Materials: Theory and Applications*, Electronic Materials: Science and Technology, ed. S. R. Rotman, Springer, Boston, MA, 1997, vol. 2.
117 M. Nikl and A. Yoshikawa, *Adv. Opt. Mater.*, 2015, **3**, 463–481.
118 Z. Xia and A. Meijerink, *Chem. Soc. Rev.*, 2017, **46**, 275–299.
119 C. W. E. Van Eijk, *Radiat. Prot. Dosim.*, 2008, **129**, 13–21.
120 P. Dorenbos, *J. Lumin.*, 2000, **91**, 155–176.
121 M. D. Birowosuto and P. Dorenbos, *Phys. Status Solidi*, 2009, **206**, 9–20.
122 P. Lecoq, A. Gektin and M. Korzhik, *Inorganic Scintillators for Detector Systems*, Springer International Publishing, Cham, 2017.
123 A. Nassalski, M. Kapusta, T. Batsch, D. Wolski, D. Mockel, W. Enghardt and M. Moszynski, in *IEEE Nuclear Science Symposium Conference Record*, IEEE, 2005, vol. 5, pp. 2823–2829.
124 B. Nucleonics, *CLLBC Scintillators High Resolution Gamma/Neutron Detectors*, **https://www.berkeleynucleonics.com/cllbc-scintillators**, accessed 11 January 2023.
125 P. Dorenbos, *J. Lumin.*, 2013, **135**, 93–104.
126 A. J. Wojtowicz, W. Drozdowski, D. Wisniewski, J. L. Lefaucheur, Z. Galazka, Z. Gou, T. Lukasiewicz and

J. Kisielewski, in *Optical Materials*, Elsevier, 2006, vol. 28, pp. 85–93.
127 M. Nikl, J. A. Mares, A. Vedda, M. Fasoli, V. Laguta, E. Mihokova, J. Pejchal, M. Zhuravleva, A. Yoshikawa and K. Nejezchleb, *IEEE Trans. Nucl. Sci.*, 2010, **57**, 1168–1174.
128 A. M. Srivastava, *J. Lumin.*, 2016, **169**, 445–449.
129 K. Kirakci, P. Kubát, K. Fejfarová, J. Martinčík, M. Nikl and K. Lang, *Inorg. Chem.*, 2016, **55**, 803–809.
130 C. W. E. van Eijk, *Phys. Med. Biol.*, 2002, **47**, R85–R106.
131 Z. Wang, C. Dujardin, M. S. Freeman, A. E. Gehring, J. E. Hunter, P. Lecoq, W. Liu, C. L. Melcher, C. L. Morris, M. Nikl, G. Pilania, R. Pokharel, D. G. Robertson, D. J. Rutstrom, S. Sjue, *et al.*, Needs, trends, and advances in scintillators for radiographic imaging and tomography, *arXiv*, 2022, preprint, arXiv.2212.10322, DOI: **10.48550/arXiv.2212.1032**.
132 P. Leblans, D. Vandenbroucke and P. Willems, *Materials*, 2011, **4**, 1034–1086.
133 S. J. Duclos, *Scintillator Phosphors for Medical Imaging*, 1998.
134 S. J. Duclos, C. D. Greskovich, R. J. Lyons, J. S. Vartuli, D. M. Hoffman, R. J. Riedner and M. J. Lynch, in *Nuclear Instruments and Methods in Physics Research, Section A: Accelerators, Spectrometers, Detectors and Associated Equipment*, North-Holland, 2003, vol. 505, pp. 68–71.
135 *Engineering of Scintillation Materials and Radiation Technologies*, ed. M. Korzhik and A. Gektin, Springer International Publishing, Cham, 2019, vol. 227.
136 C. Dujardin, E. Auffray, E. Bourret-Courchesne, P. Dorenbos, P. Lecoq, M. Nikl, A. N. Vasil'Ev, A. Yoshikawa and R. Y. Zhu, *IEEE Trans. Nucl. Sci.*, 2018, **65**, 1977–1997.
137 M. Nikl, E. Mihokova, J. Pejchal, A. Vedda, M. Fasoli, I. Fontana, V. V. Laguta, V. Babin, K. Nejezchleb, A. Yoshikawa, H. Ogino and G. Ren, *IEEE Trans. Nucl. Sci.*, 2008, **55**, 1035–1041.
138 J. Glodo, Y. Wang, R. Shawgo, C. Brecher, R. H. Hawrami, J. Tower and K. S. Shah, *Phys. Procedia*, 2017, **90**, 285–290.
139 C. Bueno, D. Albagli, J. Bendahan, D. Castleberry, C. Gordon, F. Hopkins and W. Ross, *Large area x-ray detectors for cargo radiography*, ed. T. T. Saito, D. Lehrfeld and M. J. DeWeert, 2007, p. 65401R.
140 D. Linardatos, V. Koukou, N. Martini, A. Konstantinidis, A. Bakas, G. Fountos, I. Valais and C. Michail, *Materials*, 2021, **14**, 888.
141 Rad-icon Product Family Datasheet, *Teledyne Dalsa v1.09*, 2021.
142 M. Swoboda, R. Arlt, V. Gostilo, A. Lupilov, M. Majorov, M. Moszynski and A. Syntfeld, *IEEE Trans. Nucl. Sci.*, 2005, **52**, 3111–3118.
143 *High resolution low background CeBr3 scintillators*, Product datasheet from Berkeley Nucleonics Corporation, 2021.
144 *Radiation Monitoring Devices (RMD), Development of CLYC Scintillators for Radiation Detection*, **https://www.rmdinc.com/success-story/clyc-scintillators-radiation-dete/**, accessed 11 January 2023.
145 T. Scientific, *RadEye™ SPRD-GN Spectroscopic Personal Radiation Detector*, **https://www.thermofisher.com/order/catalog/product/4250812?cid=fl-radiationsecurity?cid=fl-cad-sprdgn**, accessed 10 January 2023.
146 *Radiation Monitoring Devices (RMD), CLLBC Gamma-Neutron Scintillator*, **https://rmdinc.wpengine.com/product-category/scintillators/cllbc-gamma-neutron-scintillator/**, accessed 11 January 2023.
147 *CapeScint Macropixel MCA detector*, **https://capescint.com/new-ultra-lightweight-and-compact-scintillation-gamma-radiation-probe-sc-macropixel-mca/**.
148 *CapeSym, RadSolverTM A high energy resolution RIID*, **https://www.capesym.com/docs/RadSolver_RIID_page1.pdf**, accessed 11 January 2023.
149 J. R. Fanchi, Well Logging, *Integrated Reservoir Asset Management*, ed. J. R. Fanchi, Gulf Professional Publishing, Boston, 2010, pp. 109–124.
150 C. L. Melcher, *Nucl. Instrum. Methods Phys. Res. Sect. B Beam Interact. Mater. Atoms*, 1989, **40–41**, 1214–1218.
151 A. Nikitin and S. Bliven, *IEEE Nucl. Sci. Symp. Conf. Rec.*, 2010, 1214–1219.
152 United States Patent Office, *US Pat.*US20140319330A1, 2014.
153 United States Patent Office, *US Pat.*US20220381942A1, 2022.
154 A. G. Haus and J. E. Cullinan, *RadioGraphics*, 1989, **9**, 1203–1224.
155 R. E. D Picus, W. H. McAlister, E. Smith, S. Rodewald and R. G. Jost, *Am. J. Roentgenol.*, 1984, **143**, 1335–1338.
156 E. Seeram, *Digital Radiography*, Springer Singapore, Singapore, 2019.
157 P. Leblans, D. Vandenbroucke and P. Willems, *Materials*, 2011, **4**, 1034–1086.
158 *Superb imaging 'on the go'*, **https://medimg.agfa.com/main/superb-imaging-on-the-go/**.
159 *Dual Energy CT in Clinical Practice*, ed. T. Johnson, C. Fink, S. O. Schönberg and M. F. Reiser, Springer Berlin Heidelberg, Berlin, Heidelberg, 2011.
160 *UFC: ultra fast ceramic technology*, **https://www.siemens-healthineers.com/at/computed-tomography/technologies-innovations/ufc-ultra-fast-ceramic**.
161 H. Yamada, A. Suzuki, Y. Uchida, M. Yoshida, H. Yamamoto and Y. Tsukuda, *J. Electrochem. Soc.*, 1989, **136**, 2713–2716.
162 *C&A Japan produce GAGG:Ce 4-inch crystals*, **https://www.c-and-a.jp/assets/img/News/Ce%EF%BC%9AGAGG%204inch%E3%82%B7%E3%83%B3%E3%83%81%E3%83%AC%E3%83%BC%E3%82%BF.pdf**.
163 J. Li, X. Chen and M. Nikl, in *Processing of Ceramics: Breakthroughs in Optical Materials*, ed. A. Ikesue, John Wiley and Sons Inc., 1st edn, 2021.
164 T. Jones and D. Townsend, *J. Med. Imaging*, 2017, **4**, 011013.
165 S. Surti, A. Kuhn, M. E. Werner, A. E. Perkins, J. Kolthammer and J. S. Karp, *J. Nucl. Med.*, 2007, **48**, 471.
166 B. J. Pichler, H. F. Wehrl and M. S. Judenhofer, *J. Nucl. Med.*, 2008, **49**, 5S–23S.
167 A. Springer, *Evaluation of the quantitative accuracy of a commercially-available positron emission mammography*

scanner, University of Texas MD Anderson Cancer Center, 2010.
168 L. MacDonald, J. Edwards, T. Lewellen, D. Haseley, J. Rogers and P. Kinahan, *J. Nucl. Med.*, 2009, **50**, 1666–1675.
169 C. Ronda, in *Rare Earth Chemistry*, De Gruyter, 2020, pp. 453–462.
170 E. Shefer, A. Altman, R. Behling, R. Goshen, L. Gregorian, Y. Roterman, I. Uman, N. Wainer, Y. Yagil and O. Zarchin, *Curr. Radiol. Rep.*, 2013, **1**, 76–91.
171 M. E. Casey and D. R. Osborne, in *Advances in PET*, Springer International Publishing, Cham, 2020, pp. 71–91.
172 *GE Healthcare Introduces Omni Legend: A First-of-its-Kind All-Digital PET-CT System to Drive Efficiency, Enhance Diagnostics, and Deliver on Precision Medicine*, **https://www.ge.com/news/press-releases/ge-healthcare-introduces-omni-legend-a-first-of-its-kind-all-digital-petct-system-to**, accessed 5 January 2023.
173 D. K. Flynn-Sanders, S. -L. Chang, P. A. Thiel and R. Imbihl, *J. Vac. Sci. Technol., A*, 1992, **10**, 413–415.
174 *Phosphor Screens*, **https://www.proxivision.de/wp-content/uploads/PV_Phosphor_Screens_201601.pdf**.
175 *Phosphor Screens*, **https://scintacor.com/technologies/phosphor-screens/**, 2021.
176 R. Autrata, *Scanning Microsc.*, 1989, **3**, 739–763.
177 P. Horodysky, K. Blazek, J. Jiruse, V. Nedela, J. Spinka and M. Nikl, *New Scintillator Materials for EM*, 2019, Crytur Ltd., **https://www.crytur.com/storage/cryt_UK-General/posters%20electron%20microscopy/poster_mc_2009.pdf**.
178 *Electron Microscopy*, **https://www.crytur.com/solutions/electron-microscopy/**, accessed 22 January 2022.
179 European Patent Office, EP3492555B1, 2021.
180 M. L. McConnell, P. F. Bloser, J. Legere and J. M. Ryan, *J. Phys. Conf. Ser.*, 2016, **763**, 012008.
181 J. E. Grove, C. C. Cheung, M. Kerr, L. J. Mitchell, B. F. Phlips, R. S. Woolf, E. A. Wulf, M. S. Briggs, C. A. Wilson-Hodge and D. P. Kocevski, *Glowbug, a low-cost, high-sensitivity gamma-ray burst telescope*, 2020.
182 L. Mitchell, B. F. Phlips, R. S. Woolf, T. T. Finne and N. Johnson, in *UV, X-Ray, and Gamma-Ray Space Instrumentation for Astronomy XXI*, ed. O. H. Siegmund, SPIE, 2019, p. 17.
183 *PROBA2's EUV Imager for Solar Corona Detection*, **https://scintacor.com/proba2s-euv-imager-for-solar-corona-detection/**.
184 *SWAP electronics | PROBA2 Science Center*, **https://proba2.sidc.be/about/SWAP/electronics**, accessed 21 January 2023.
185 T. Sharma, P. F. Bloser, J. S. Legere, C. M. Bancroft, C. Frost, M. L. McConnell and J. M. Ryan, *2019 IEEE Nucl. Sci. Symp. Med. Imaging Conf. NSS/MIC* 2019, DOI: **10.1109/NSS/MIC42101.2019.9059725**.
186 M. Julien, J. M. Ryan, P. F. Bloser, J. S. Legere, C. M. Bancroft, M. L. McConnell, R. M. Kippen and S. Tornga, in *2012 IEEE Nuclear Science Symposium and Medical Imaging Conference Record (NSS/MIC)*, 2012, pp. 1893–1900.
187 *JAXA | X-ray Astronomy Satellite "Suzaku" Completes Scientific Mission*, **https://global.jaxa.jp/press/2015/08/20150826_suzaku.html**, accessed 22 January 2023.
188 M. Kokubun, K. Abe, Y. Ezoe, Y. Fukazawa, S. Hong, H. Inoue, T. Itoh, T. Kamae, D. Kasama, M. Kawaharada, N. Kawano, K. Kawashima, S. Kawasoe, Y. Kobayashi, J. Kotoku, M. Kouda, A. Kubota, G. M. Madejski, K. Makishima, T. Mitani, H. Miyasaka, R. Miyawaki, K. Mori, M. Mori, T. Murakami, M. M. Murashima, K. Nakazawa, H. Niko, M. Nomachi, M. Ohno, Y. Okada, K. Oonuki, G. Sato, M. Suzuki, H. Takahashi, I. Takahashi, T. Takahashi, K. Tamura, T. Tanaka, M. Tashiro, Y. Terada, S. Tominaga, S. Watanabe, K. Yamaoka, T. Yanagida and D. Yonetoku, *IEEE Trans. Nucl. Sci.*, 2004, **51**, 1991–1996.
189 P. Ubertini, F. Lebrun, G. Di Cocco, A. Bazzano, A. J. Bird, K. Broenstad, A. Goldwurm, G. La Rosa, C. Labanti, P. Laurent, I. F. Mirabel, E. M. Quadrini, B. Ramsey, V. Reglero, L. Sabau, B. Sacco, R. Staubert, L. Vigroux, M. C. Weisskopf and A. A. Zdziarski, *Astron. Astrophys.*, 2003, **411**, L131–L139.
190 V. Scotti and G. Osteria, *Nucl. Part. Phys. Proc.*, 2017, **291–293**, 118–121.
191 V. Scotti and G. Osteria, The high energy particle detector onboard the CSES satellite, *2016 IEEE Nuclear Science Symposium, Medical Imaging Conference and Room-Temperature Semiconductor Detector Workshop (NSS/MIC/RTSD)*, Strasbourg, France, 2016, pp. 1–8, DOI: **10.1109/NSSMIC.2016.8069878**.
192 V. Bharadwaj, M. Brock, B. Heing, R. Miro and N. Mukarram, *U.S. Intellectual Property and Counterfeit Goods-Landscape Review of Existing/Emerging Research*, Washington, D.C., 2020.
193 OECD and European Union Intellectual Property Office, *Trends in Trade in Counterfeit and Pirated Goods*, OECD, Paris, 2019.
194 World Health Organization, *A study on Public Health and Socio-economic Impact of Substandard and Falsified*, Medical Products, Geneva, 2020.
195 J. Gooch, B. Daniel, V. Abbate and N. Frascione, *TrAC, Trends Anal. Chem.*, 2016, **83**, 49–54.
196 O. Guillou, C. Daiguebonne, G. Calvez and K. Bernot, *Acc. Chem. Res.*, 2016, **49**, 844–856.
197 F. Adams and C. Barbante, *Compr. Anal. Chem.*, 2015, **69**, 339–384.
198 Luminescence - Sun Chemical Security, Solutions, **https://luminescence-scs.com/solutions**.
199 Honeywell, Fluorescent Pigments & Taggants, **https://prod-edam.honeywell.com/content/dam/honeywell-edam/pmt/oneam/en-us/authentication-technologies/documents/Lumilux-SafetySecurityPigments-Brochure.pdf**.
200 Olnica, Olnica Taggant, **https://olnica.com/system/olnica-invisible-taggant**.
201 R. Judson and R. Porter, *Estimating the Worldwide Volume of Counterfeit U.S. Currency: Data and Extrapolation*, Washington, D.C., 2003.
202 Interpol, Counterfeit currency and security documents.

203 R. Arppe and T. J. Sørensen, *Nat. Rev. Chem.*, 2017, **1**, 1–13.
204 M. R. Carro-Temboury, R. Arppe, T. Vosch and T. J. Sørensen, *Sci. Adv.*, 2018, **4**, e1701384.
205 K. Binnemans, *Coord. Chem. Rev.*, 2015, **295**, 1–45.
206 J. C. G. Bünzli and S. V. Eliseeva, *Chem. Sci.*, 2013, **4**, 1939–1949.
207 J. F. Suyver and A. Meijerink, *Chem. Weekbl.*, 2002, **98**, 12–13.
208 H. Kohlmann, in *Chemistry of the Elements*, German Chemical Society (GDCh), 2019, pp. 148–150.
209 K. Binnemans and D. Moors, *J. Mater. Chem.*, 2002, 3374–3376.
210 United States Patent Office, *US Pat.*US20200354596A1, 2018.
211 S. Biju, Y. K. Eom, J. C. G. Bünzli and H. K. Kim, *J. Mater. Chem. C*, 2013, **1**, 3454–3466.
212 M. Xiao and P. R. Selvin, *J. Am. Chem. Soc.*, 2001, **123**, 7067–7073.
213 S. Susumu and W. Masanobu, *Bull. Chem. Soc. Jpn.*, 1970, **43**, 1955–1962.
214 R. A. Gudmundsen, O. J. Marsh and E. Matovich, *J. Chem. Phys.*, 1964, **39**, 272–274.
215 F. R. G. e Silva, J. F. S. Menezes, G. B. Rocha, S. Alves, H. F. Brito, R. L. Longo and O. L. Malta, *J. Alloys Compd.*, 2000, **303–304**, 364–370.
216 R. Brennetot and J. Georges, *Spectrochim. Acta Mol. Biomol. Spectrosc.*, 2000, **56**, 703–715.
217 H. Zhang, H. Song, B. Dong, L. Han, G. Pan, X. Bai, L. Fan, S. Lu, H. Zhao and F. Wang, *J. Phys. Chem. C*, 2008, **112**, 9155–9162.
218 S. Wen, X. Zhang, L. Yao, M. Xi, L. Zhang, H. Fong and L. Liu, *J. Mater. Chem. C*, 2013, **1**, 1613–1617.
219 The Danish Patent and Trademark Office, DK2718395T3, 2012.
220 R. Vijayakumar and X. Huang, *J. Mater. Sci. Mater. Electron.*, 2019, **30**, 4196–4202.
221 S. Rahim, M. H. Hasim, M. T. M. Ayob, I. A. Rahman, K. A. M. Salleh and S. Radiman, *Mater. Res.*, 2020, **22**, 20190383.
222 L. Ozawa and M. Itoh, *Chem. Rev.*, 2003, **103**, 3835–3856.
223 United States Patent Office, *US Pat.*US10337689B2, 2018.
224 European Patent Office, EP3050850B1, 2014.
225 S. Ekambaram and K. C. Patil, *J. Alloys Compd.*, 1997, **248**, 7–12.
226 G. Blasse and A. Bril, *Philips Res. Rep.*, 1968, **23**, 201–206.
227 European Patent Office, EP3050857A1, 2016.
228 European Patent Office, EP2021861B1, 2007.
229 S. Yang, C. Stoffers, F. Zhang, S. M. Jacobsen, B. K. Wagner, C. J. Summers and N. Yocom, *Appl. Phys. Lett.*, 1998, **72**, 158.
230 Z. Xinmin, W. Hao, Z. Heping and S. Qiang, *J. Rare Earths*, 2007, **25**, 701–705.
231 Taiwan Intellectual Property Office, TW200944577A, 2005.
232 J. M. Kim, K. N. Kim, S. H. Park, J. K. Park, C. H. Kim and H. G. Jang, *J. Korean Chem. Soc.*, 2005, **49**, 201–207.
233 V. Bachmann, C. Ronda and A. Meijerink, *Chem. Mater.*, 2009, **21**, 2077–2084.
234 United States Patent Office, *US Pat.*US7229573B2, 2004.
235 European Patent Office, EP3338023B1, 2016.
236 Official Tourism Website of the Republic of Colombia, Colombia's currency information.
237 D. Kim, S. Park, S. H. Park, B. C. Choi, J. H. Kim and J. H. Jeong, *Mater. Res. Bull.*, 2018, **107**, 280–285.
238 J. Cui, L. Wang, Q. Shi, Y. Tian, P. Huang and C. Cui, *Polyhedron*, 2018, **141**, 284–288.
239 Taiwan Intellectual Property Office, TWI374176B, 2004.
240 R. Won, *Nat. Mater.*, 2010, **9**, S13.
241 United States Patent Office, *US Pat.*US3711262A, 1970.
242 S. Babani, A. A. Bature, M. I. Faruk and N. K. Dankadai, *Int. J. Tech. Res. Appl.*, 2014, **2**, 59–63.
243 M. E. Fermann and I. Hartl, *IEEE J. Sel. Top. Quantum Electron.*, 2009, **15**, 191–204.
244 A. D. Ellis and F. C. Garcia Gunning, *IEEE Photon. Technol. Lett.*, 2005, **17**, 504–506.
245 D. Keck, *IEEE J. Sel. Top. Quantum Electron.*, 2000, **6**, 1254–1258.
246 United States Patent Office, *US Pat.*US10429589B2, 2018.
247 D. A. Ackerman, J. E. Johnson, L. J. P. Ketelsen, L. E. Eng, P. A. Kiely and T. G. B. Mason, in *Optical Fiber Telecommunications IV-A*, ed. I. P. Kaminow and T. Li, Academic Press, Cambridge, Fourth., 2002, pp. 587–665.
248 K. Grobe, in *Handbook of Fiber Optic Data Communication*, ed. C. DeCusatis, Academic Press, Cambridge, Fourth., 2013, pp. 85–122.
249 J. C. G. Bünzli, *Trends Chem*, 2019, **1**, 751–762.
250 Y. Sun, A. K. Srivastava, J. Zhou and J. W. Sulhoff, *Bell Labs Tech. J.*, 1999, **4**, 187–206.
251 B. N. Samson, P. A. Tick and N. F. Borrelli, *Opt. Lett.*, 2001, **26**, 145–147.
252 United States Patent Office, *US Pat.*US9831635B2, 2016.
253 United States Patent Office, *US Pat.*US11509110B2, 2020.
254 United States Patent Office, *US Pat.*US5005175A, 1989, pp. 12–14.
255 United States Patent Office, *US Pat.*US11509109B2, 2020.
256 China National Intellectual Property Administration, CN101896845A, 2009.
257 S. Tanabe, *Compt. Rendus Chem.*, 2002, **5**, 815–824.
258 R. J. Mears, L. Reekie, I. M. Jauncey and D. N. Payne, *Electron. Lett.*, 1987, **23**, 1026–1028.
259 S. V. Eliseeva and J.-C. G. Bünzli, *New J. Chem.*, 2011, **35**, 1165–1176.
260 United States Patent Office, *US Pat.*US4963832A, 1989.
261 Japan Patent Office, JP3884744B2, 2004.
262 M. A. Ali, A. F. Elrefaie, R. E. Wagner and S. A. Ahmed, *J. Light. Technol.*, 1996, **14**, 1436–1448.
263 Y. Durteste, M. Monerie, J. Y. Allain and F. Poignant, *Electron. Lett.*, 1991, **27**, 626–628.
264 United States Patent Office, *US Pat.*US8897644B2, 2012.
265 United States Patent Office, *US Pat.*US5378664A, 1993.
266 Y. Nishida, M. Yamada, T. Kanamori, K. Kobayashi, J. Temmyo, S. Sudo and Y. Ohishi, *IEEE J. Quantum Electron.*, 1998, **34**, 1332–1339.
267 J.-C. G. Bünzli and S. V. Eliseeva, *J. Rare Earths*, 2010, **28**, 824–842.

268 United States Patent Office, *US Pat.*US6337944B1, 1999.
269 R. Min, X. Hu, L. Pereira, M. Simone Soares, L. C. B. Silva, G. Wang, L. Martins, H. Qu, P. Antunes, C. Marques and X. Li, *Opt. Laser Technol.*, 2022, **147**, 107626.
270 Y. Zheng, J. Pearson, R. H. C. Tan, W. P. Gillin and P. B. Wyatt, *J. Mater. Sci. Mater. Electron.*, 2009, **20**, 430–434.
271 L. Song, J. Hu, J. Wang, X. Liu and Z. Zhen, *Photochem. Photobiol. Sci.*, 2008, **7**, 689–693.
272 United States Patent Office, *US Pat.*US11114815B1, 2017.
273 D. Zhang, C. Chen, D. Zheng, T. Li, L. Song and Z. Zhen, *Appl. Phys. Lett.*, 2009, **94**, 041119.
274 J. C. G. Bünzli and A. S. Chauvin, *Lanthanides in solar energy conversion*, 2014, vol. 44.
275 Z. Li, B. Zhang, Z. Zhang, J. Bünzli, A. R. bin Mohd Yusoff, Y. Noh and P. Gao, *Mater. Sci. Eng. R Rep.*, 2023, **152**, 100710.
276 R. A. S. Ferreira, S. F. H. Correia, A. Monguzzi, X. Liu and F. Meinardi, *Mater. Today*, 2020, **33**, 105–121.
277 World Intellectual Property Organization, WO2014136115A1, 2014.
278 J. Sun, X. Yang, S. Sun, L. Zhao, S. Wang and Y. Li, *Inorg. Chem. Commun.*, 2022, **143**, 109731.
279 China National Intellectual Property Administration, CN108878554B, 2008.
280 G. Brito-Santos, B. Gil-Hernández, C. Hernández-Rodríguez, B. González-Díaz, R. Guerrero-Lemus and J. Sanchiz, *Mater. Sci. Eng., B*, 2023, **288**, 116207.
281 P. Weitz, V. M. Le Corre, X. Du, K. Forberich, C. Deibel, C. J. Brabec and T. Heumüller, *Adv. Energy Mater.*, 2023, **13**, 2202564.
282 O. Essahili, M. Ouafi and O. Moudam, *Sol. Energy*, 2022, **245**, 58–66.
283 R. A. S. Ferreira, A. N. C. Neto, S. F. H. Correia and L. D. Carlos, in *Modern Applications of Lanthanide Luminescence*, ed. A. de Bettencourt-Dias, Springer, Cham, Cham, 2023, vol. 19, pp. 1–33.
284 United States Patent Organization, *US Pat.*US4367367A, 1979.
285 United States Patent Organization, *US Pat.*US11329180B2, 2014.
286 Korean Intellectual Property Office, KR101150702B1, 2011.
287 United States Patent Organization, *US Pat.*US10982136B2, 2017.
288 China National Intellectual Property Administration, CN212517224U, 2020.
289 World Intellectual Property Organization, WO2009151679A3, 2009.
290 United States Patent Office, *US Pat.*US8637763B2, 2010.
291 United States Patent Office, *US Pat.*US7928317B2, 2007.
292 Ana de Bettencourt-Dias, *Modern Applications of Lanthanide Luminescence*, 2023, vol. 19.
293 J. M. Meijer, L. Aarts, B. M. Van Der Ende, T. J. H. Vlugt and A. Meijerink, *Phys. Rev. B: Condens. Matter Mater. Phys.*, 2010, **81**, 035107.
294 China National Intellectual Property Administration, CN113667427A, 2021.
295 China National Intellectual Property Administration, CN217881538U, 2022.
296 R. Candanosa, *Growing Green on the Red Planet - American Chemical Society*, **https://www.acs.org/content/acs/en/education/resources/highschool/chemmatters/past-issues/2016-2017/april-2017/growing-green-on-the-red-planet.html**.
297 I. Monostori, M. Heilmann, G. Kocsy, M. Rakszegi, M. Ahres, S. B. Altenbach, G. Szalai, M. Pál, D. Toldi, L. Simon-Sarkadi, N. Harnos, G. Galiba and É. Darko, *Front. Plant Sci.*, 2018, **9**, 605.
298 Y. Ma, A. Xu and Z. M. (Max) Cheng, *Hortic. Plant J.*, 2021, **7**, 552–564.
299 C. Marondedze, X. Liu, S. Huang, C. Wong, X. Zhou, X. Pan, H. An, N. Xu, X. Tian and A. Wong, *Hortic. Res.*, 2018, **5**, 68.
300 *Passenger Train Emergency Systems II*, Published online 2009, **https://www.federalregister.gov/documents/2012/01/03/2011-33103/passenger-train-emergency-systems-ii**.
301 *DHi Nearing Goal Line In Installation of Pentagon Photoluminescent Safety Marking Systems*, **https://www.dh-inc.com/archive/35-dhi-nearing-goal-line-in-pentagon-pl-installation**, accessed 12 February 2023.
302 United States Patent Office, *US Pat.* US8479423B2, 2012.
303 Defense Holdings, Inc. Delivers 550 Safe, Green, AfterGlow® Photoluminescent EXIT Signs To Replace Radioactive Tritium EXIT Signs At Fort Monmouth, *Bus Wire*, Published online May 2011, **https://www.businesswire.com/news/home/20110513005034/en/Defense-Holdings-Inc.-Delivers-550-Safe-Green-AfterGlow®-Photoluminescent-EXIT-Signs-To-Replace-Radioactive-Tritium-EXIT-Signs-At-Fort-Monmouth**.
304 J. Botterman and P. F. Smet, *Opt. Express*, 2015, **23**, A868–A881.
305 J. Xu and S. Tanabe, *J. Lumin.*, 2019, **205**, 581–620.
306 D. Poelman, D. Van der Heggen, J. Du, E. Cosaert and P. F. Smet, *J. Appl. Phys.*, 2020, **128**, 240903.